Geochemistry Geophysics Geosystems G3
AN ELECTRONIC JOURNAL OF THE EARTH SCIENCES
Published by AGU and the Geochemical Society

Article
Volume 7, Number 7
27 July 2006
Q07011, doi:10.1029/2005GC001178
ISSN: 1525-2027

Heat flow variations on a slowly accreting ridge: Constraints on the hydrothermal and conductive cooling for the Lucky Strike segment (Mid-Atlantic Ridge, 37°N)

Francis Lucazeau, Alain Bonneville, and Javier Escartin
Géosciences Marines, IPGP-CNRS, 4 Place Jussieu, F-75252 Paris Cedex 05, France (lucazeau@ipgp.jussieu.fr)

Richard P. Von Herzen
Woods Hole Oceanographic Institution, Woods Hole, Massachusetts 02543, USA

Philippe Gouze
Laboratoire de Géophysique et d'Hydrodynamique en Forage, ISTEEM - cc 56, 4 Place Eugène Bataillon, F-34095 Montpellier Cedex, France

Hélène Carton and Mathilde Cannat
Géosciences Marines, IPGP-CNRS, 4 Place Jussieu, F-75252 Paris Cedex 05, France

Valérie Vidal
Géosciences Marines, IPGP-CNRS, 4 Place Jussieu, F-75252 Paris Cedex 05, France

Now at Laboratoire de Physique, Ecole Normale Supérieure de Lyon, 46 Allée d'Italie, F-69364 Lyon Cedex 07, France

Claudia Adam
Géosciences Marines, IPGP-CNRS, 4 Place Jussieu, F-75252 Paris Cedex 05, France

Now at Institute for Research on Earth Evolution, Japan Agency for Marine-Earth Science and Technology, 2-15 Natsushima, Yokosuka, 237-0061, Japan

[1] We report 157 closely spaced heat flow measurements along the Lucky Strike segment in the Mid-Atlantic Ridge (MAR) for ages of the ocean floor between 0 and 11 Ma. On the eastern flank of a volcanic plateau delimiting off-axis and axial domains, the magnitude of heat flow either conforms to the predictions of conductive lithospheric cooling models or is affected by localized anomalies. On the western flank it is uniformly lower than conductive model predictions. We interpret the observed patterns of heat flow by lateral fluid circulation in a highly permeable oceanic basement. The circulation geometries are probably 3-D rather than 2-D and are determined by the configuration of the basement/sediment interface and the distribution of effectively unsedimented seamounts where water recharge can occur. Two major hydrothermal circulation systems can possibly explain the observations off-axis: the first would involve lateral pore water flow from west to east, and the second would have a reverse flow direction. The wavelengths and magnitudes of heat flow anomalies require Darcy velocities of the order of 1–4 m/year, which are similar to those proposed for fast-accreted crust elsewhere. However, a large proportion of this MAR domain remains unaffected by hydrothermal cooling, which is a relatively unusual observation but

confirms the validity of conductive thermal models for seafloor ages between 5 and 10 Ma. Closer to the ridge axis (<5 Myr old crust), water circulation affects the overall axial domain, as larger proportions of basement are exposed. As much as 80–90% of the heat flux from the axial domain may be transferred to the Lucky Strike vent field, in agreement with the estimated discharge.

Components: 13,889 words, 17 figures, 1 table.

Keywords: heat flow; Mid-Atlantic Ridge.

Index Terms: 3015 Marine Geology and Geophysics: Heat flow (benthic); 3017 Marine Geology and Geophysics: Hydrothermal systems (0450, 1034, 3616, 4832, 8135, 8424); 3035 Marine Geology and Geophysics: Midocean ridge processes.

Received 7 November 2005; **Revised** 12 April 2006; **Accepted** 2 May 2006; **Published** 27 July 2006.

Lucazeau, F., A. Bonneville, J. Escartin, R. P. Von Herzen, P. Gouze, H. Carton, M. Cannat, V. Vidal, and C. Adam (2006), Heat flow variations on a slowly accreting ridge: Constraints on the hydrothermal and conductive cooling for the Lucky Strike segment (Mid-Atlantic Ridge, 37°N), *Geochem. Geophys. Geosyst.*, *7*, Q07011, doi:10.1029/2005GC001178.

1. Introduction

[2] Heat flow measured at the ocean floor has been the subject of many discussions regarding its relative importance with respect to that of hydrothermal flow in the upper crust near the ridge axis. The discrepancy between surface measurements and values predicted by conductive models such as Half-Space Cooling (HSC) or plate models [*Sclater and Francheteau*, 1970; *Parsons and Sclater*, 1977; *Stein and Stein*, 1992] indicate that hydrothermal circulation can redistribute heat flow in oceanic basins [*Lister*, 1972]. Heat flow values in young crust, presumably affected by such hydrothermal circulation, are mostly lower than or equal to the conductive values, and only rarely higher, suggesting that discharge areas may be focused at basement exposures where conventional heat flow measurements are not possible. Recent studies have confirmed such localized discharge at seamounts associated with high heat flow values [*Davis et al.*, 1989; *Thomson et al.*, 1995; *Villinger et al.*, 2002; *Fisher et al.*, 2003; *Wheat et al.*, 2004].

[3] However, the mechanisms and the magnitude of hydrothermal circulation are still a matter of debate. Statistical comparison between measured and theoretical heat flow has been used by *Stein and Stein* [1994] to assess that the process is important only in ocean floor younger than 65 Myr, after which heat would be primarily conducted, rather than advected, through the seafloor. The magnitude of the hydrothermal component has been determined at the same time by *Pelayo et al.* [1994], on the basis of magma chambers and earthquakes depths at mid-ocean ridges. Nevertheless, there exist several sites where hydrothermal circulation has been deduced for ocean-floor older than 65 Myr [*Embley et al.*, 1983; *Von Herzen*, 2004], and conversely, others where heat flow lies close to values predicted by conductive cooling models for ocean floor younger than 65 Myr [*Anderson et al.*, 1979; *Langseth et al.*, 1988; *Davis et al.*, 1999]. Other factors such as sediment thickness [*Sclater*, 2003] or density of seamount [*Villinger et al.*, 2002] are probably as important as the age of the crust as an influence on hydrothermal ventilation.

[4] A robust alternative to characterize the importance of hydrothermal circulation relies on a combination of evenly spaced heat flow measurements and collocated seismic profiles along segments of the ocean floor. Several of these studies carried out at fast spreading ridges [*Williams et al.*, 1974; *Green et al.*, 1981; *Davis et al.*, 1992; *Villinger et al.*, 2002; *Fisher et al.*, 2003] show that heat flow ranges between about 20–50% of the value predicted by conductive models when the age of ocean floor is older than 1–2 Ma. In the context of slow spreading ridges, where only a few such high resolution studies exist, there is off-axis evidence of hydrothermal circulation at 20 Ma [*Langseth and Herman*, 1981] and at 80 Ma [*Embley et al.*, 1983]. *Williams et al.* [1977] have also reported heat flow measurements affected by hydrothermal circulation in close proximity to the ridge axis, at the termination of a ridge segment near the Famous transform fault and within the rift valley floor. This study may not be representative of the overall thermal state and hydrothermal circulation of a slow-spreading segment, as it is limited to one nodal basin.

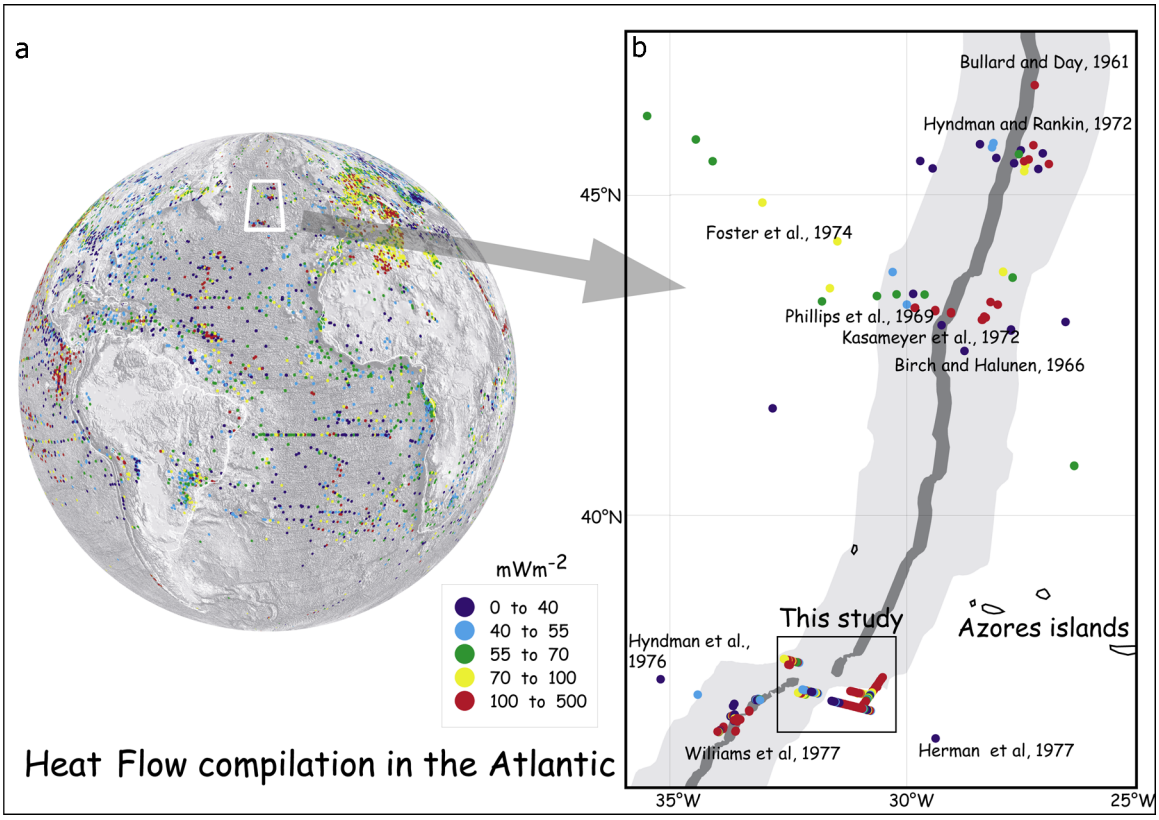

Figure 1. (a) Global heat flow data set (modified from *Pollack et al.* [1993]) with focus on the Atlantic Ocean. (b) The right part is a close-up view on Azores region. The light gray area corresponds to ocean floor younger than 10 Myr; the dark gray area corresponds roughly to the axial valley domain.

[5] Since existing measurements are probably not representative of the overall thermal state of the Mid-Atlantic Ridge (MAR), additional measurements in other locations are still necessary for improved understanding. The LUCKYFLUX experiment was designed to carry out a high-density heat flow measurement survey in the vicinity of a slow-spreading segment, and in crust <10 Myr old where heat flow values predicted by the models vary most rapidly. 157 new measurements are used to evaluate the thermal regime of this slow-spreading segment, and the distribution of heat flow anomalies and quantification of hydrothermal flow in the upper oceanic crust.

2. Geological Framework

[6] The Lucky Strike segment and hydrothermal vent field are located along the Mid-Atlantic Ridge (MAR, 37–38°N) southwest of the Azores islands. This section of the ridge is influenced by the Azores hot spot and its activity since at least 25 Ma [*Cannat et al.*, 1999; *Gente et al.*, 2003]. As a consequence, this section of the MAR shows a regional topographic gradient, deepening away from the Azores islands (40 °N), and associated with regional crustal thickness variations [*Detrick et al.*, 1995]. This area is characterized by V-shaped ridges that are the result of the ridge/hot spot interaction [*Cannat et al.*, 1999; *Escartín et al.*, 2001], which modified spatially and temporally the amount of crustal melting. The excess melt produced a thick crust (up to 14 km near Azores islands) and an associated elevated plateau of about 10–5 Ma in age. During the ridge/hot spot interaction, the tectonic activity was reduced (lack of normal faulting) but numerous seamounts were produced. Later on (~5 Ma), the plateau was rifted to form a series of ridge segments, including the Lucky Strike segment that hosts several hydrothermal fields, and "normal" seafloor spreading started again. The off-axis volcanic ridges are important physiographic features, locally rising to <300 meters below seafloor, that define a near-axis domain (within the V-shaped ridges) and an off-axis domain (outside of the V-shaped ridges).

[7] The Lucky Strike vent field, located at the summit of a central volcano, is one of the loci of the MOMAR (Monitoring the Mid-Atlantic Ridge) research program, and the LUCKYFLUX experiment has been implemented in this framework to

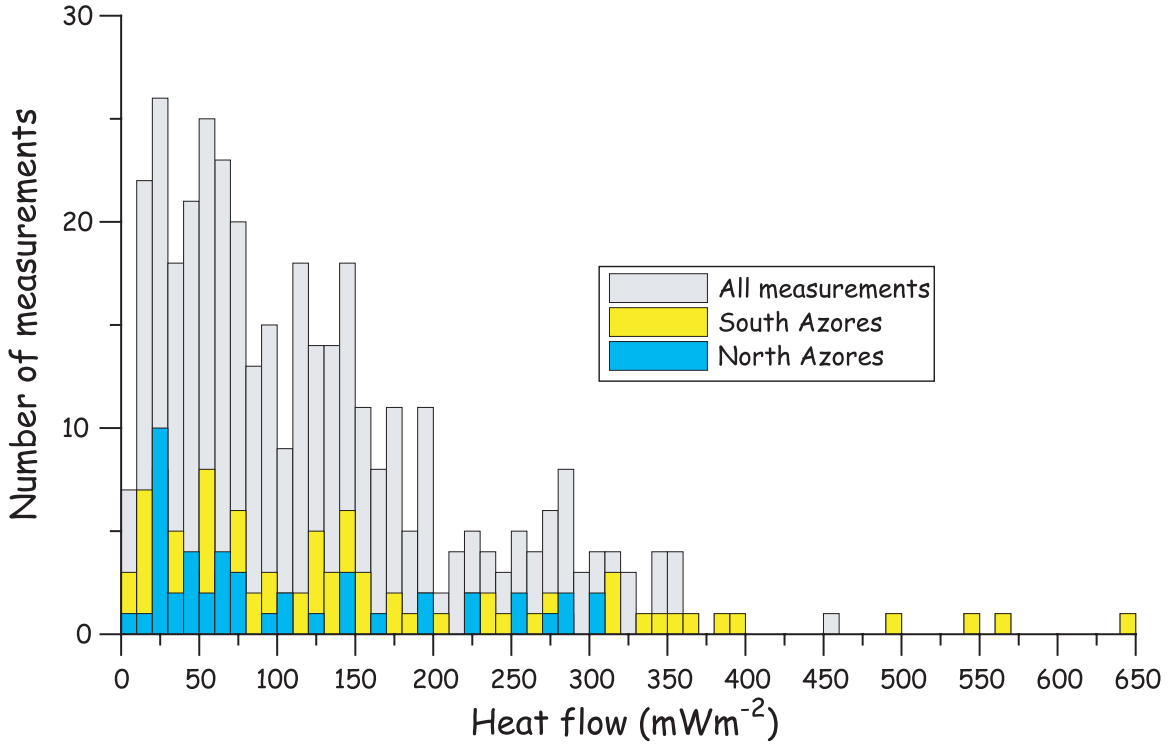

Figure 2. Histogram of published heat flow values in the Atlantic for seafloor age <10 Ma.

provide regional and local constraints to the hydrothermal vent field at the segment center.

3. Previous Heat Flow Measurements in the Atlantic

[8] Since the first Atlantic heat flow measurements published by *Bullard* [1954] in a deep oceanic basin offshore Ireland, a total of about 2500 additional measurements have been obtained (Figure 1a). The first heat flow measurements in the near-axis domain recorded low values, which were interpreted at the time as precluding continental drift [*Langseth et al.*, 1966]. Since that study, the number of near-axis measurements has not increased very much and in the last published heat flow compilation [*Pollack et al.*, 1993], there are less than 400 measurements in the MAR for age of seafloor between 0 and 10 Ma (62 in the southern hemisphere and 326 in the northern hemisphere). Most of the measurements in the northern hemisphere (Figure 1b) have been obtained in the vicinity of the Azores islands [*Bullard and Day*, 1961; *Birch and Halunen*, 1966; *Phillips et al.*, 1969; *Hyndman and Rankin*, 1972; *Kasameyer et al.*, 1972; *Foster et al.*, 1974; *Hyndman et al.*, 1976; *Williams et al.*, 1977]. These data show a large number of low values and a large dispersion (Figure 2), which are common characteristics of hydrothermal perturbations. However, several studies have been carried out near fracture zones [*Phillips et al.*, 1969; *Kasameyer et al.*, 1972; *Foster et al.*, 1974; *Hyndman et al.*, 1976; *Williams et al.*, 1977] where the extreme topography and the proximity to a segment end within the vicinity of an adjacent older plate may result in fluid circulation and an anomalous thermal regime.

[9] Because of the small number of near-axis values, the peculiar environments where they have been obtained and the rather old techniques involved, the data set quality in the Atlantic is probably not as good as for the Pacific spreading centers where recent measurements have been obtained [*Davis et al.*, 1992; *Villinger et al.*, 2002]. Therefore the LUCKYFLUX experiment, which represents more than 1/3 of all data previously acquired in the Atlantic for this age range and includes areas with thick sediment cover (~100 meters or more), can provide newer evidence to understand detailed heat transfer mechanisms of a slow spreading ridge system.

4. Distribution of Measurements and Data Processing

[10] Heat flow measurements (Figure 3) were located along several seismic lines approximately

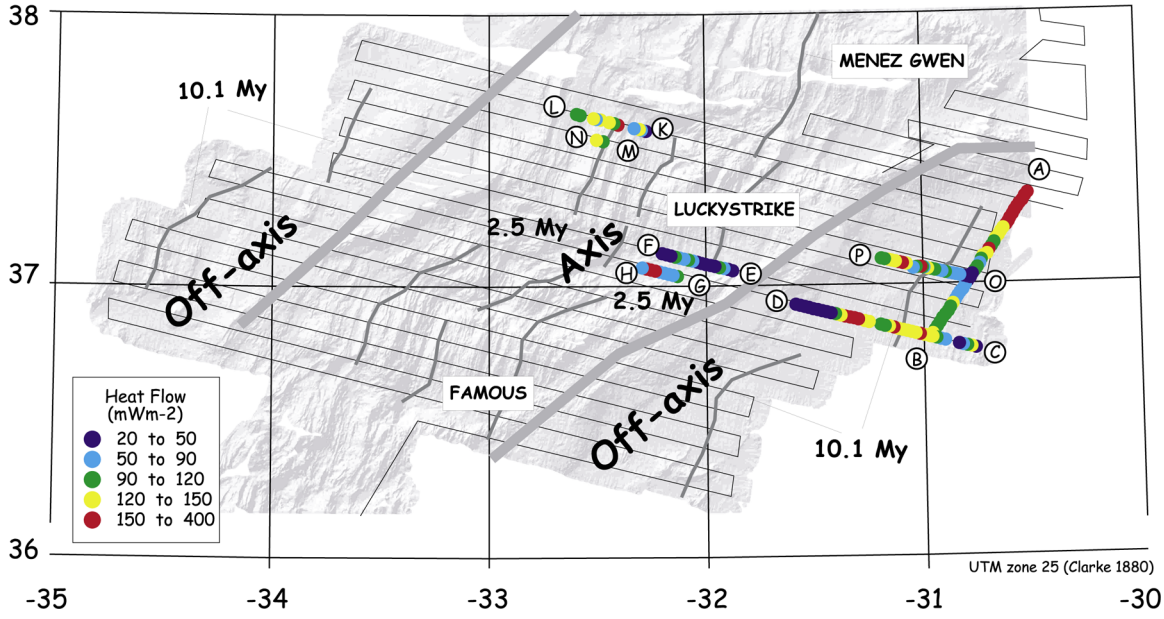

Figure 3. Location of heat flow measurements (color dots) on a shaded map of topography. Axial domain, anomaly 2A (2.5 Myr), and anomaly 5 (10.1 Myr) [*Cannat et al.*, 1999] are also represented. Thick gray lines represent the location of the volcanic plateaus' maximum gravity low. Thin lines indicate the location of previous seismic lines: profiles CD, EF, GH, KL, and MN coincide with seismic lines, whereas profile OP is located halfway.

parallel to the spreading direction (~N100E), in addition to a profile (profile AB) sub parallel to and nearly coincident with the 10 Ma isochron (An5). The seismic lines have been obtained during a previous survey (SUDAÇORES experiment [*Cannat et al.*, 1999]) and extend up to 165 km from the ridge axis with a spacing of about 8 km (Figure 3). The seismic device consisted of two GI guns of 45/45 and 105/105 cubic inch capacities providing a broadband source, and a 6-channel streamer with a maximum offset of 450 m, and positioning was obtained with GPS throughout the cruise. The lines have been reprocessed for the present study, including the following steps: sorting into common midpoint gathers, predictive deconvolution to attenuate the first seafloor multiple, stacking (using a constant velocity of 1800 m/s), and water-velocity Stolt migration, which allow collapse of diffraction hyperbolae associated with strong scattering at the top of the oceanic crust. The resulting time sections have a lateral resolution of 25 m and a vertical resolution of about 30 m in the uppermost layer (sediments). Although the seismic source was not very powerful, the topography of the basement/sediment interface is satisfactorily imaged (Figures 6, 7, 8, 10, 11, and 12). However, because of their spacing (8 km), interpolation of sediment thickness across these lines provides a map of low resolution only (Figure 8). Except profile AB, which is orthogonal to seismic lines, and profile OP, which is offset by 4 km, all other profiles are coincident with seismic lines. As both seismic and heat flow surveys were done using GPS navigation, the greatest uncertainty in the position of heat flow measurements and seismic profiles arises from that of the position of the heat flow probe with respect to the ship, and is estimated to about 100 m.

[11] Owing to time limitations, off-axis heat flow profiles (outside the V-shaped ridge) were only conducted on the East flank of the ridge (profiles AB, CD and OP), and extending to the outer limits of the volcanic plateaus that form the V-shaped ridges. The near axis profiles (within the V-shaped ridge) extend from the ridgeward limit of the V-shaped ridge toward the edge of the axial rift valley (EF and GH on the South-East and KL and MN on the North-West). The inner profiles have been carried out preferentially in the outer corner of ridge-non-transform offset intersections, where the sediment thickness is greatest.

[12] We used a ~five meter long cylindrical probe with seven outrigger thermistors and line heaters, allowing in situ measurements of the temperature and the thermal conductivity of sediments [*Von Herzen*, 1987]. Deviation of the probe from vertical was determined from a micro-processor device combining tilt measurements in two orthogonal directions. The water pressure (depth) and temper-

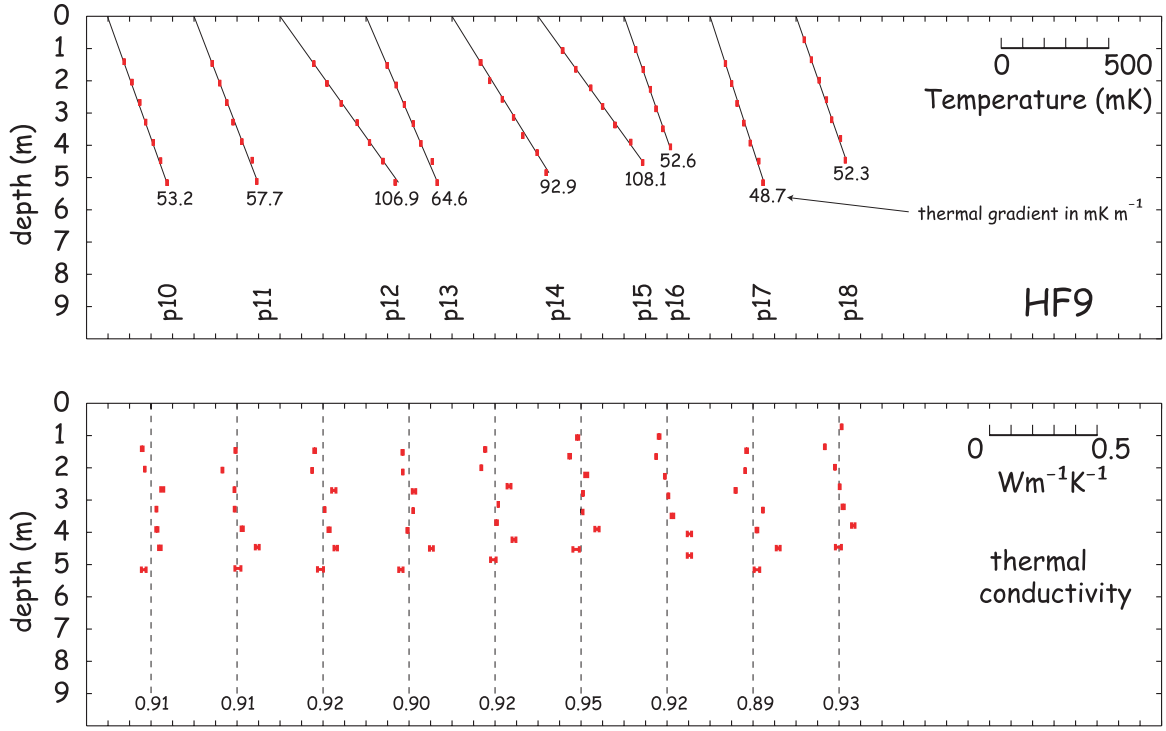

Figure 4. Examples of (top) thermal gradients and (bottom) thermal conductivity determinations obtained for the LUCKYFLUX station HF 9.

ature (T_i) variables were each sampled at 12 second intervals. The precision of temperature measurements obtained with this instrument exceeds 1 mK. The data acquisition sequence includes measurements of in situ temperatures during five minutes after probe penetration, followed by the temperature evolution during continuous heating of the sensor probes to determine thermal conductivity of the sediments. First, we calculate the equilibrium temperature at each thermistor by a linear extrapolation of the temperature evolution with the inverse of time so as to correct for the frictional heating induced by the penetration. Second, we determine the temperature gradient interactively by a linear best fit to the equilibrium temperatures calculated for each of the thermistors. Third, we determine the thermal conductivity at each thermistor and a site conductivity value. And fourth, we calculate the heat flow from the determined temperature gradient after tilt correction and from the site thermal conductivity. Each step is associated with an error analysis. The data reduction procedure is explained extensively by *Bonneville et al.* [1993].

[13] Heat flow measurements have been systematically corrected for topographic and sedimentation effects. Topographic corrections are related to the perturbations caused by an uneven topography on the near-surface isotherms. Sedimentation corrections are related to the transient perturbation caused by the accumulation of cold sediments. More details on these corrections are given in Appendix A, but they are usually small, except where local relief is large. A heat refraction correction, related to conductivity contrast between sediment and basement, cannot be applied systematically because the resolution of seismic lines (separated each others by 8 km) is not sufficient, but it can be shown (see Appendix A) that some specific geometries and conductivity contrasts can create high amplitude and small-wavelength anomalies.

[14] Temperature gradients are mostly linear (Figure 4; all temperature and conductivity profiles are available at http://www.ipgp.jussieu.fr/~bonneville/heat-flow/luckyflux/), which excludes significant seasonal sea-bottom temperature variations and/or percolation of fluids through sediments. However, as we recorded water-bottom temperatures, we can observe local anomalies on profile CD possibly related to local fluid venting (see details in Appendix A and Figure 6), but with no consequence on the gradient linearity at the site surveyed.

Table 1 (Representative Sample). Location of Measurements and Associated Information[a] [The full Table 1 is available in the HTML version of this article at http://www.g-cubed.org]

Profile	ST	P	Longitude °	Longitude ′	Latitude °	Latitude ′	Depth, m	Pen, m	Tilt, deg	Twat, mK	nG	Grad, mK/m	σG	nK	K, W/m/K	σK	HF, mW/m^2	σHF	Distance, km	Age, Ma	Sed Thick, s TWT	Topo Corr, mW/m^2	Sed Corr	Corr Heat Flow, mW/m^2
	1	**2**	−30	30.64	37	19.72	2237	2.7	6		2	166.8	1	0	1.01	0.02	**168.5**	3.5	0.0	7.7		0.0		**168.5**
AB																								
AB	**1**	**3**	−30	31.42	37	18.96	2245	5.1	1	3.34	2	161.2	0.5	0	1.01	0.02	**162.8**	3.3	1.8	8.2		−1.5		**161.3**
AB	**1**	**4**	−30	32.09	37	18.01	2257	5	7	3.29	2	186.8	1.9	0	1.01	0.02	**188.7**	4.2	3.8	8.9	0.483	−0.8	20.39	**208.3**
AB	**1**	**5**	−30	32.92	37	17.30	2265	4.7	6	3.33	2	164.5	2.6	0	1.01	0.02	**166.1**	4.2	5.6	9.4	0.490	−0.2	17.67	**183.5**
AB	**1**	**6**	−30	33.61	37	16.57	2248	4.8	21	3.3	2	169.5	8.5	0	1.01	0.02	**171.2**	9.2	7.3	9.9	0.475	5.1	17.29	**193.6**
AB	**1**	**7**	−30	34.31	37	15.77	2276	3.8	14	3.3	2	161.9	4.8	0	1.01	0.02	**163.5**	5.8	9.1	10.1	0.460	−2.3	15.93	**177.2**
AB	**1**	**8**	−30	34.90	37	14.93	2313	4.6	9	3.26	2	180.5	2.3	0	1.01	0.02	**182.3**	4.3	10.9	10.2	0.427	−10.4	16.64	**188.5**
AB	**1**	**9**	−30	35.55	37	14.11	2274	4.6	0	3.26	2	173.1	2.9	0	1.01	0.02	**174.8**	4.5	12.7	10.3	0.415	10.3	15.52	**200.6**
AB	**1**	**10**	−30	36.09	37	13.39	2308	4.4	16	3.26	2	159.1	2.2	0	1.01	0.02	**160.7**	3.9	14.2	10.3	0.392	2.1	13.62	**176.4**
AB	**1**	**11**	−30	36.69	37	12.67	2334	4.6	7	3.26	3	162.1	3.9	0	1.01	0.02	**163.7**	5.1	15.8	10.4	0.369	4.0	13.14	**180.8**
AB	**2**	**1**	−30	37.52	37	11.94	2371	5.2	1	3.26	6	148	6	5	0.96	0.03	**142.1**	7.7	17.6	10.4	0.353	−1.2	11	**151.9**
AB	**2**	**2**	−30	38.29	37	11.20	2388	4.7	7	3.2	6	139.4	6.4	6	0.96	0.03	**134.4**	7.5	19.4	10.5	0.339	2.6	10.02	**147.1**
AB	**2**	**3**	−30	38.93	37	10.33	2429	5.1	13	3.19	7	129.6	5.1	6	0.98	0.02	**127.1**	5.5	21.3	10.5	0.327	−1.3	9.2	**135.0**
AB	**2**	**4**	−30	39.69	37	9.64	2464	5.2	9	3.14	7	124.7	3.4	6	0.98	0.03	**122.8**	4.6	23.0	10.6	0.313	−1.6	8.54	**129.8**
AB	**2**	**5**	−30	40.21	37	8.89	2496	5	8	3.14	7	112	3.1	6	0.98	0.04	**109.7**	5.4	24.5	10.6	0.304	1.7	7.44	**118.9**
AB	**2**	**6**	−30	40.86	37	8.04	2596	5.2	5	3.12	7	104.7	3.2	6	0.99	0.02	**103.7**	3.7	26.4	10.7	0.294	−7.8	6.81	**102.7**
AB	**2**	**7**	−30	41.61	37	7.29	2594	5.2	16	3.09	7	151.4	6.9	6	1.06	0.04	**159.7**	9.3	28.2	10.8	0.269	−3.1	9.71	**166.3**
AB	**2**	**8**	−30	42.16	37	6.40	2623	4.7	24	3.05	7	140.7	4.6	6	0.97	0.03	**135.8**	5.7	30.0	10.8	0.184	−0.6	6.02	**141.3**
AB	**2**	**9**	−30	43.28	37	5.73	2652	5.2	14	3.04	7	103.4	6.2	6	0.98	0.02	**101.7**	6.6	32.0	10.9	0.218	−3.4	5.17	**103.5**
AB	**2**	**10**	−30	43.89	37	5.13	2652	5.2	16	3.05	7	100.1	3.9	6	0.97	0.02	**97.4**	4.2	33.4	10.9	0.274	−4.5	5.98	**98.9**
AB	**3**	**1**	−30	47.66	37	0.41	2615	5.2	8	3.05	7	80	3.2	6	0.95	0.05	**76.2**	5.2	43.7	11.0	0.359	1.3	5.82	**83.3**
AB	**3**	**2**	−30	48.37	36	59.59	2610	5.2	29	3.03	6	97.1	2.3	6	0.93	0.04	**90.6**	4.0	45.6	11.0	0.392	−0.9	7.44	**97.2**
AB	**3**	**3**	−30	49.11	36	58.58	2578	3.8	25	3.02	7	101.8	5.4	6	0.92	0.03	**93.9**	5.9	47.8	11.1	0.460	1.3	8.74	**103.9**
AB	**3**	**4**	−30	49.85	36	57.95	2570	5.2	14	3	6	48.9	2.3	6	1.02	0.02	**50.0**	2.5	49.3	11.1	0.449	0.5	4.56	**55.1**
AB	**3**	**5**	−30	50.50	36	57.20	2590	5.2	1	2.99	7	35.2	1.9	6	0.94	0.04	**33.1**	2.3	51.0	11.2	0.452	−0.2	3.02	**35.9**
AB	**4**	**1**	−30	47.66	37	0.41	2615	5.2	22	2.99	6	37.6	2.3	4	0.99	0.04	**37.1**	2.7	43.7	11.3	0.434	0.0	3.26	**40.4**
AB	**4**	**2**	−30	48.37	36	59.59	2610	5.2	17	3.03	7	66.4	3.3	4	0.97	0.06	**64.1**	4.9	45.6	11.4	0.402	−0.2	5.28	**69.2**
AB	**4**	**3**	−30	49.11	36	58.58	2578	4.6	21	3.06	7	90.1	3.1	4	0.98	0.04	**87.9**	5.0	47.8	11.5	0.325	2.4	6.06	**96.4**
AB	**4**	**4**	−30	49.85	36	57.95	2570	5.2	19	3.07	7	59.4	3.1	4	0.98	0.03	**58.1**	3.6	49.3	11.6	0.278	2.1	3.51	**63.7**
AB	**4**	**5**	−30	50.50	36	57.20	2590	5.2	11	3.08	7	51.9	2	4	0.98	0.03	**51.1**	2.6	51.0	11.6	0.242	−0.2	2.75	**53.7**
AB	**4**	**6**	−30	51.14	36	56.36	2607	4.9	8	3.08	7	66.1	4	4	0.99	0.04	**65.6**	4.7	52.9	11.7	0.271	−0.4	3.86	**69.0**
AB	**4**	**7**	−30	51.88	36	55.53	2612	5.1	18	3.07	7	133.6	5.5	4	0.98	0.04	**130.6**	7.1	54.7	11.8	0.337	−2.3	9.16	**137.4**
AB	**4**	**8**	−30	52.59	36	54.70	2597	5.2	16	3.06	7	102.1	2.9	4	0.98	0.03	**100.0**	4.4	56.6	11.9	0.385	2.9	7.78	**110.7**
AB	**4**	**9**	−30	53.22	36	53.86	2632	4.9	24	3.06	7	104.9	4.6	4	0.98	0.04	**102.9**	5.9	58.4	12.0	0.370	−0.6	7.72	**110.1**

[a] ST, station number; P, penetration number for that station; Depth, water depth; Pen, penetration depth; Tilt, probe inclination; Twat, water bottom temperature, nG, number of thermistors used for gradient estimate, Grad, temperature gradient; σG, standard error on gradient; nK, number of conductivity determinations; K, average conductivity; σK, standard error on conductivity; HF, uncorrected heat flow; σHF, standard error on heat flow; distance, distance to the ridge axis (except for profile AB); age, age of ocean floor (interpolated from *Cannat et al.* [1999]), Sed thick, sediment thickness; Topo Corr, topographic correction; Sed Corr, sediment correction (Hutchinson model); Corr Heat Flow, heat corrected for sedimentation and topography.

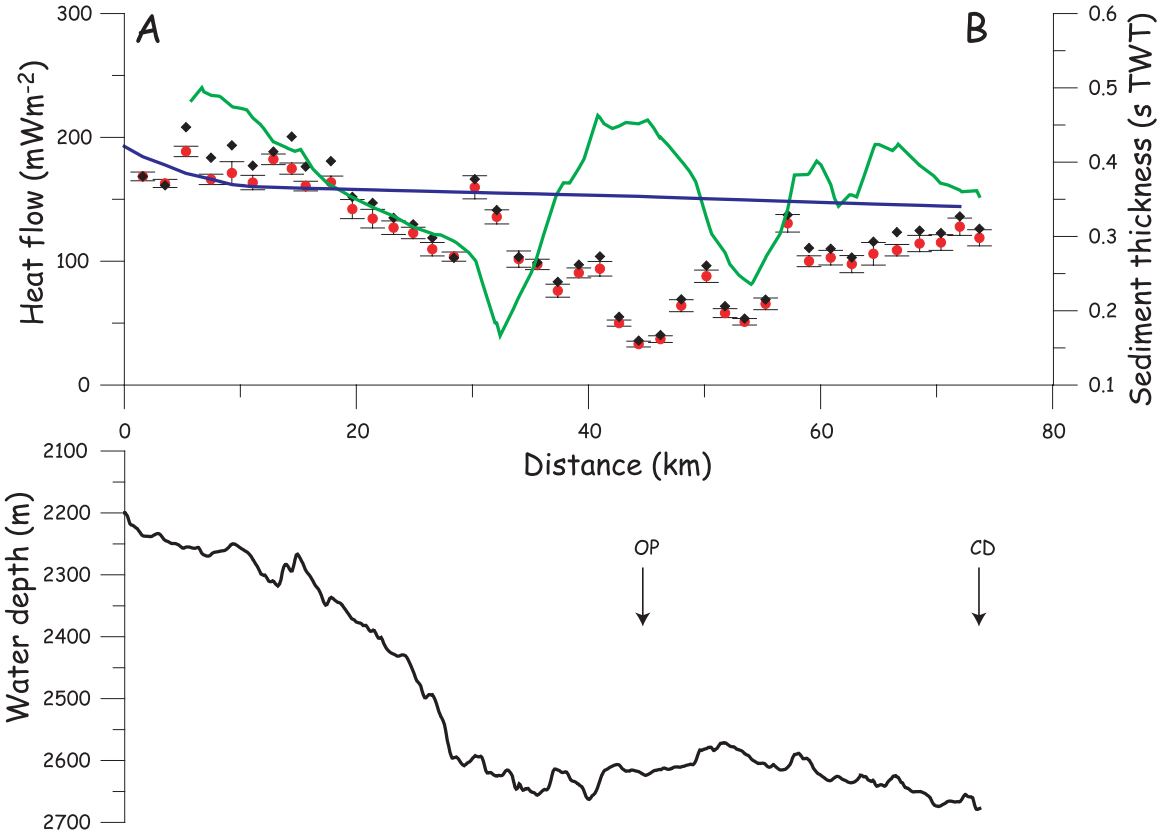

Figure 5. Heat flow measurements (uncorrected values represented by red dots with associated standard errors, and corrected values for topographic and sedimentation effects represented by black diamonds) along profile AB. Blue line is heat flow inferred from conductive reference HSC. Green line to sediment thickness. North is on the left side of the profile. Intersections with heat flow profiles OP and CD are located by the arrows on the water depth profile.

[15] Raw and corrected data are given in Table 1. Measurements have been obtained with probe tilts up to 40° or more, although most of them are less than 15°. Temperature profiles are generally linear, and in 115 penetrations the thermal gradients are determined with more than 5 thermistors, and the heat flow was determined in 111 penetrations also with more than 5 thermistors. For 23 penetrations, heating did not start and conductivity was estimated from the closest in-situ measurements instead: as conductivities measured in the Lucky Strike area are rather homogeneous (average = 0.97 $Wm^{-1}K^{-1}$; standard deviation = 0.05 $Wm^{-1}K^{-1}$ for N = 126 determinations), the error introduced in the calculation of heat flow should not be very important. The quality of the heat flow measurements is therefore good, and a maximum of 37 penetrations can be considered of lower quality owing to limitations on either the thermal gradient determination (fewer than 3 thermistors), the conductivity measurements (no in-situ values), or the excessive probe tilt (>25° for some of the measurements).

5. Results

[16] We present the results from the off-axis and near-axis domain independently, as they are separated by the volcanic plateaus associated with the propagating V-shaped ridges, over which no heat flow measurements were obtained. Owing to the differences in the nature and thickness of sediment, most heat flow penetrations were successful in the off-axis domain, whereas near-axis profiles are incomplete because of unsatisfactory probe penetrations.

5.1. Off-Axis Domain

[17] We obtained three profiles (Figure 3), one parallel to isochrons (AB) and two in the orthog-

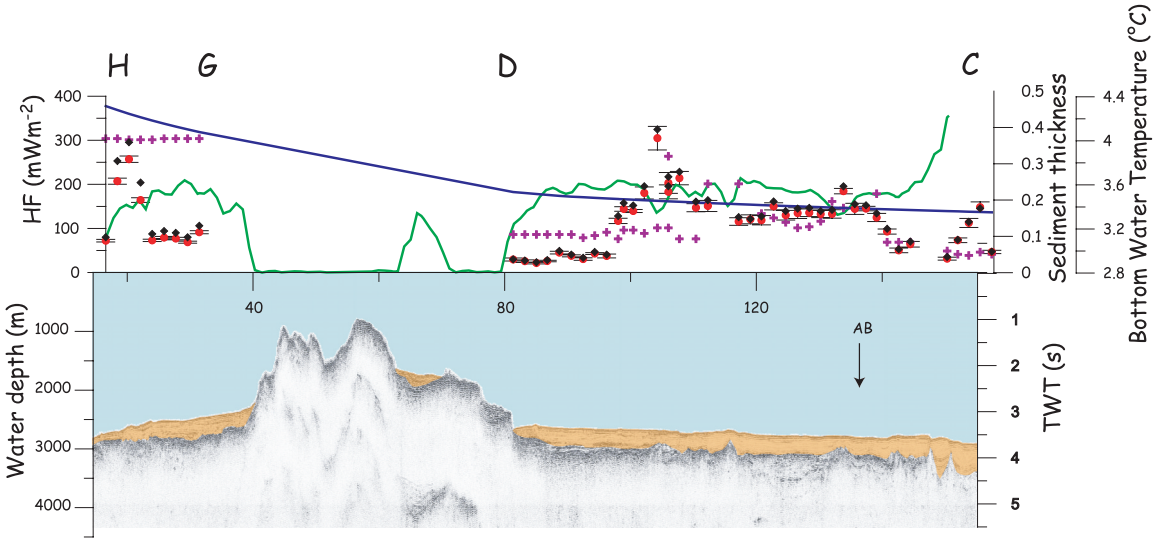

Figure 6. Heat flow measurements (uncorrected, red dots; corrected for topography and sedimentation, black diamonds), HSC conductive model (blue line), sediment thickness (green line), and seismic profile (sediment cover in yellow) as a function of distance to the ridge axis for profiles CD and GH. Bottom water temperatures are reported as purple crosses: They are remarkably uniform in the near-axis domain, while they show variations in the off-axis domain that could be related to similar variations of heat flow. Intersection with heat flow profile AB is located by the arrow on the seismic section.

onal direction along flow lines (CD and OP), which show a complex pattern of heat flow.

5.1.1. Along-Isochron Profile

[18] Profile AB, nearly coincident with isochron 5 (~10.1 Ma) [*Cannat et al.*, 1999], shows large variations in heat flow with values ranging from <50 to >200 mW/m^2 (Figure 3). Heat flow values are in good agreement with conductive models in the northern part, where the bathymetry is the shallowest. Toward the south, there is a broad 20-km wide heat flow minimum centered about 45 km (Figure 5), corresponding to a zone with thicker sediment cover. Sediment thickness shows two minima (30 and 55 km, Figure 5) that are each associated with a local heat flow high and low, respectively.

5.1.2. Along-Flow Line Profiles

[19] Profiles CD and OP extend from the eastern edge of the V-shaped ridge, and intersect the along-isochron profile AB further east (Figure 4). Only profile CD shows heat flow values that are close to the conductive models predictions over a 30 km section (110 to 140 km in Figure 6), while overall lower values are measured in proximity to the edge of the V-shaped ridge and at the crossing with profile AB in this same profile (140 km in Figure 6). Profile OP (Figure 7) shows instead overall low heat flow values relative to conductive models, except for the western extremity near the V-shaped ridge flank, where they tends to the conductive cooling models values. Local anomalous heat flow peaks are found at both profiles. The peak in profile OP (118 km, Figure 7) is associated with an adjacent basement outcrop immediately to the north, which is not imaged by the seismic profile offset by about 4 km from the heat flow line. Basement highs are also associated with short wavelength heat flow highs in profile CD at 104 and 133 km (Figure 6). As discussed previously, high amplitude very short wavelength conductive anomalies are possibly associated with seamounts: it is therefore unlikely that such anomalies as those observed at 120 km on profile OP and at 105 km on profile CD are related to heat refraction only, but surely reflect convective ventilation.

5.1.3. Global Pattern

[20] The sediment map (Figure 8), interpolated from the digitized sediment thickness along seismic lines, shows the relative differences between measured heat flow and the conductive cooling models. A large number of these values are not significantly different (within ±20%) from the conductive model. There exist also several positive anomalies (heat flow higher than the conductive predictions), generally with short wavelengths and two negative anomalies (heat flow lower than the

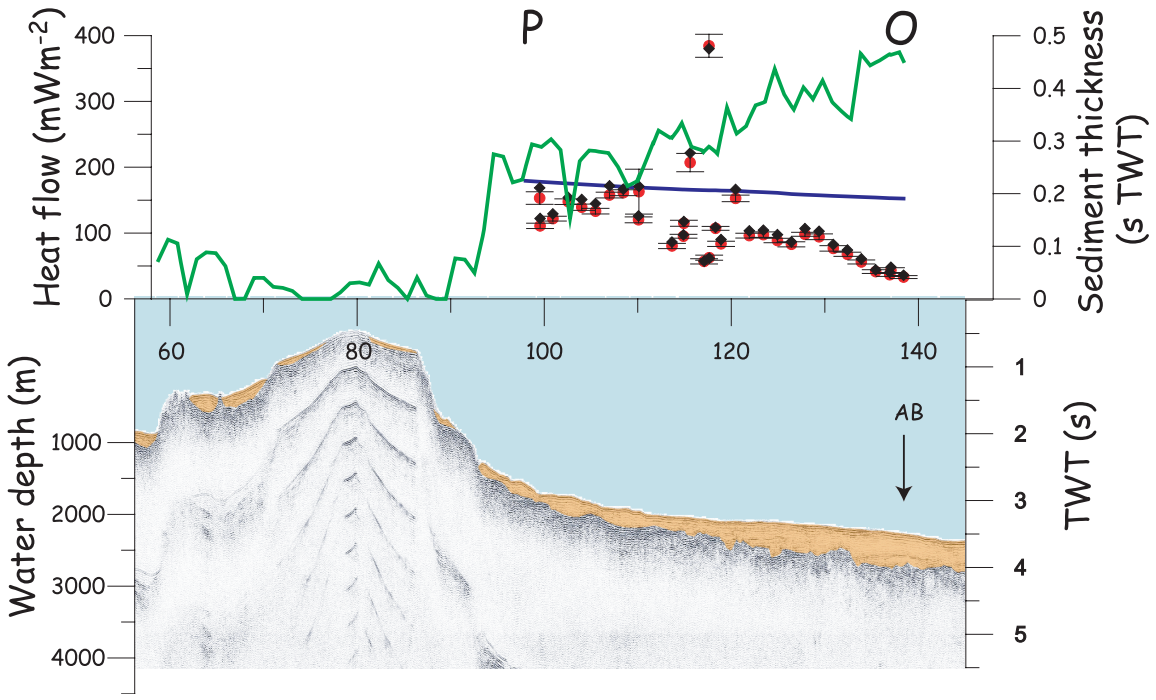

Figure 7. Heat flow measurements (red dots), HSC conductive model (blue line), sediment thickness (green line), and seismic profile (sediment cover in yellow) as a function of distance to the ridge axis for profile OP. Intersection with heat flow profile AB is located by the arrow on the seismic section.

conductive predictions) with greater wavelengths. Heat flow higher than surrounding values is observed in several places where basement ridges are buried (locations 1, 3, 6, and 10 in Figure 8). In other cases, buried ridges are located where penetrations failed (locations 2 and 4 in Figure 8) and might correspond to similar anomalies. These features have however very short wavelengths (~1 km). Other features of much larger extension have on the other hand no relationship with sediment thickness: western ends of profiles CD and OP are in the same structural position, but heat flow is 75–100% lower than the conductive cooling model on profile CD where sediment thickness is greater and is rather normal with respect to this model on profile OP where sediment thickness is less important. A similar observation can be made at the intersection of profiles AB and OP, where sediment thickness cover appears complete and several hundred meters thick and heat flow is locally lower than surrounding values.

[21] However, spacing of seismic lines (~8 km) is probably too large for imaging small seamounts, such as that observed on line OP at 115 km (Figure 7). Therefore we have reported the same heat flow anomalies on the detailed bathymetry map (Figure 9), which can provide a detailed image of seamount structure and also extend the domain covered by seismic profiles. It becomes clear that the heat flow anomalies are all located near basement exposures, but conversely the latter are not necessarily associated with heat flow anomalies. The two largest anomalies are negative and located near large basement exposures: on the eastern flank of the volcanic plateau for profile CD and on the western side of a large seamount for profile OP (in the eastern corner of Figure 9). The positive heat flow anomalies are usually isolated, with two exceptions at 105 km on profile CD and at 120 km on profile OP.

5.2. Axial Domain

[22] We made four heat flow profiles in the axial domain (within the V-shaped ridge) along flow lines, where sediments are observed on seismic profiles (Figures 6, 10, 11, and 12). All profiles are thus located along the Northwest and Southeast outside corners of the ridge-offset intersections, where the crust is more depressed and the sediment cover thickest (Figure 3). However, probe penetration was poor, especially in the Northwest, owing to the different nature of the sediment cover and the presence of rocks or gravel that caused damage to the probe and the thermistors (only 3 successful

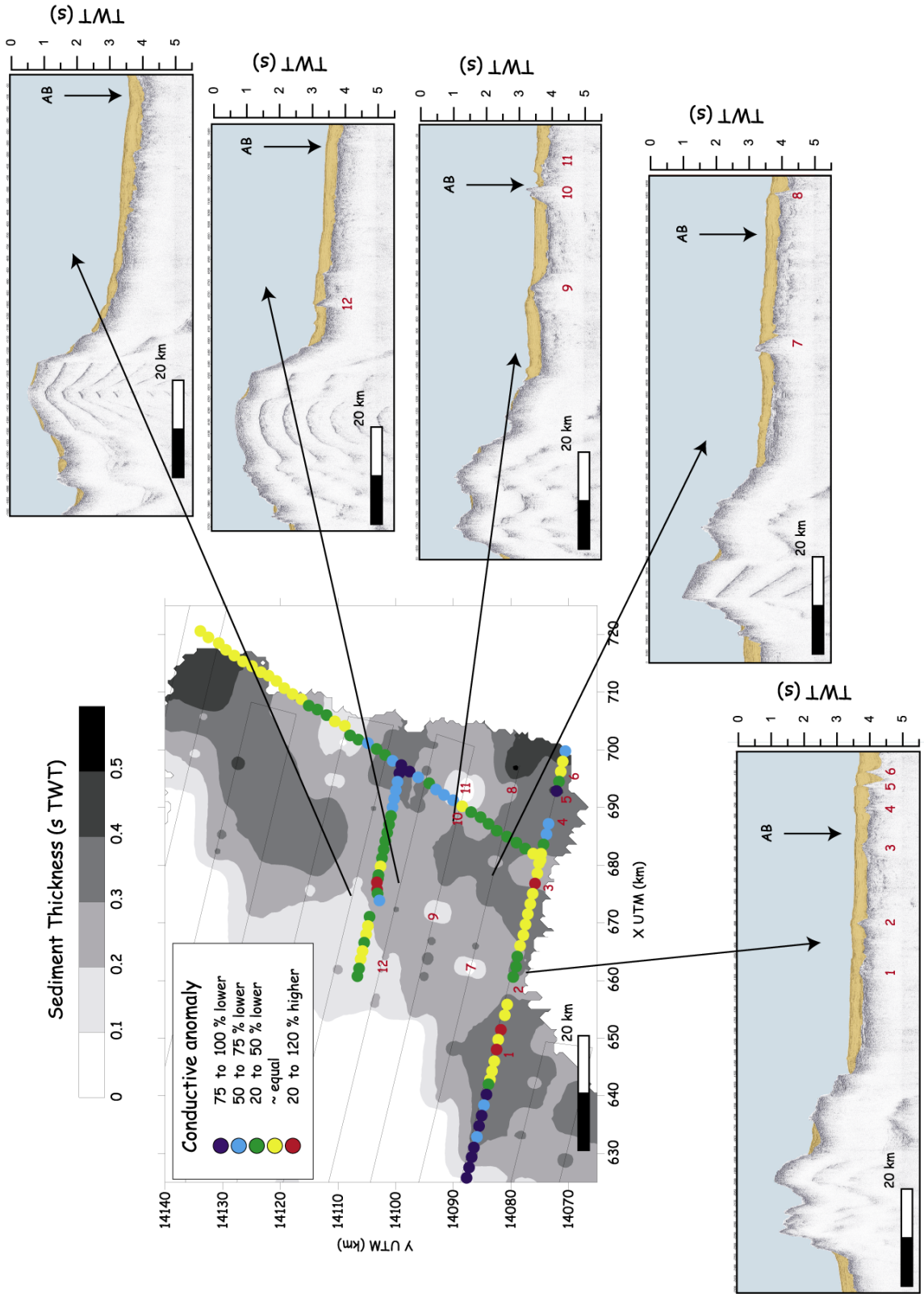

Figure 8. Interpolated sediment thickness map and seismic profiles available in the area of off-axis measurements (scale in kilometers). Heat flow anomaly with respect to HSC conductive reference and location of seismic lines are also indicated on the map. Intersections with heat flow profile AB are located by the arrow on seismic sections.

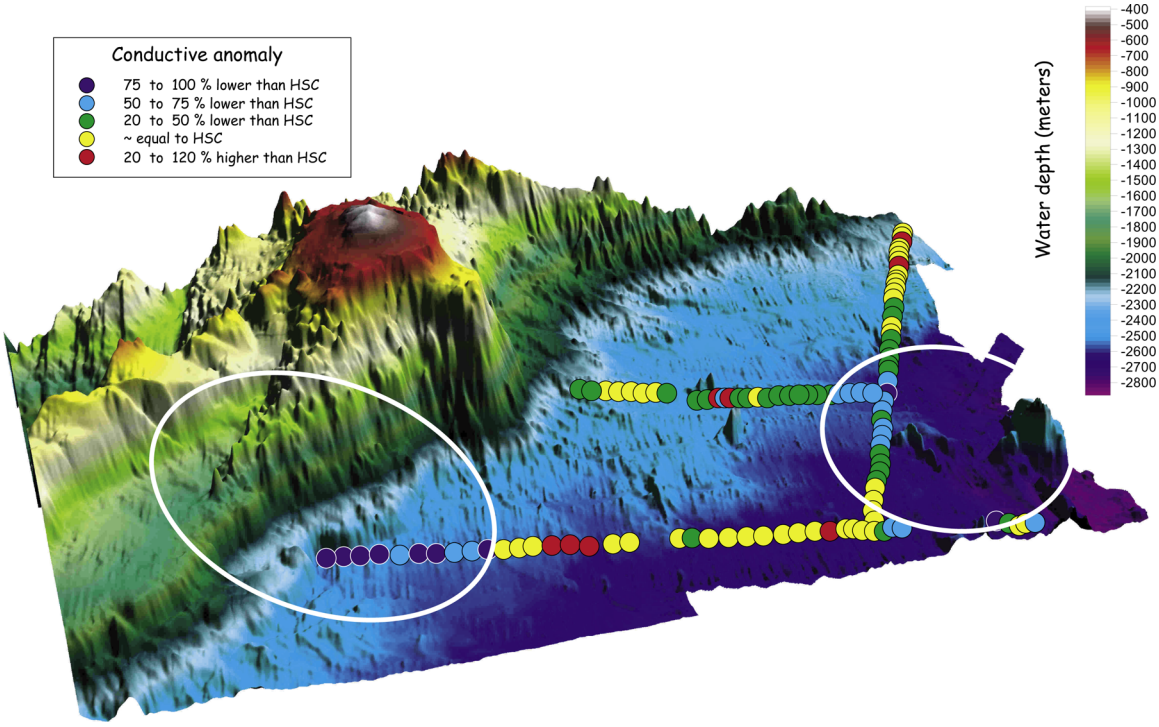

Figure 9. Three-dimensional view of the three profiles located off-axis. A color circle at each point represents the magnitude of the conductive anomaly, defined as the difference between HF measurements and HF predicted by HSC (normalized by HSC). Yellow circles are equal to the predicted value (with a range of ±20%). White ellipses correspond more or less to the two identified hydrothermal systems.

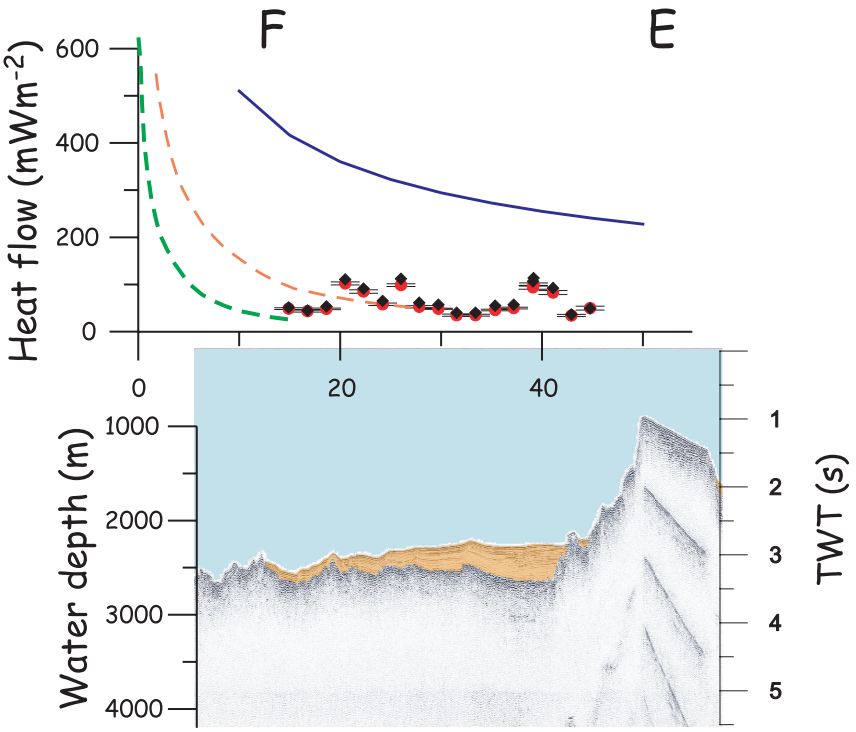

Figure 10. Heat flow measurements (red dots), heat flow corrected for topography and sedimentation (diamonds), HSC conductive model (blue line), Chen and Morgan model (1 cm/year accretion: dashed green line and 3 cm/year accretion: dashed orange line), and seismic profile (sediment cover in yellow) as a function of distance to the ridge axis for profiles EF.

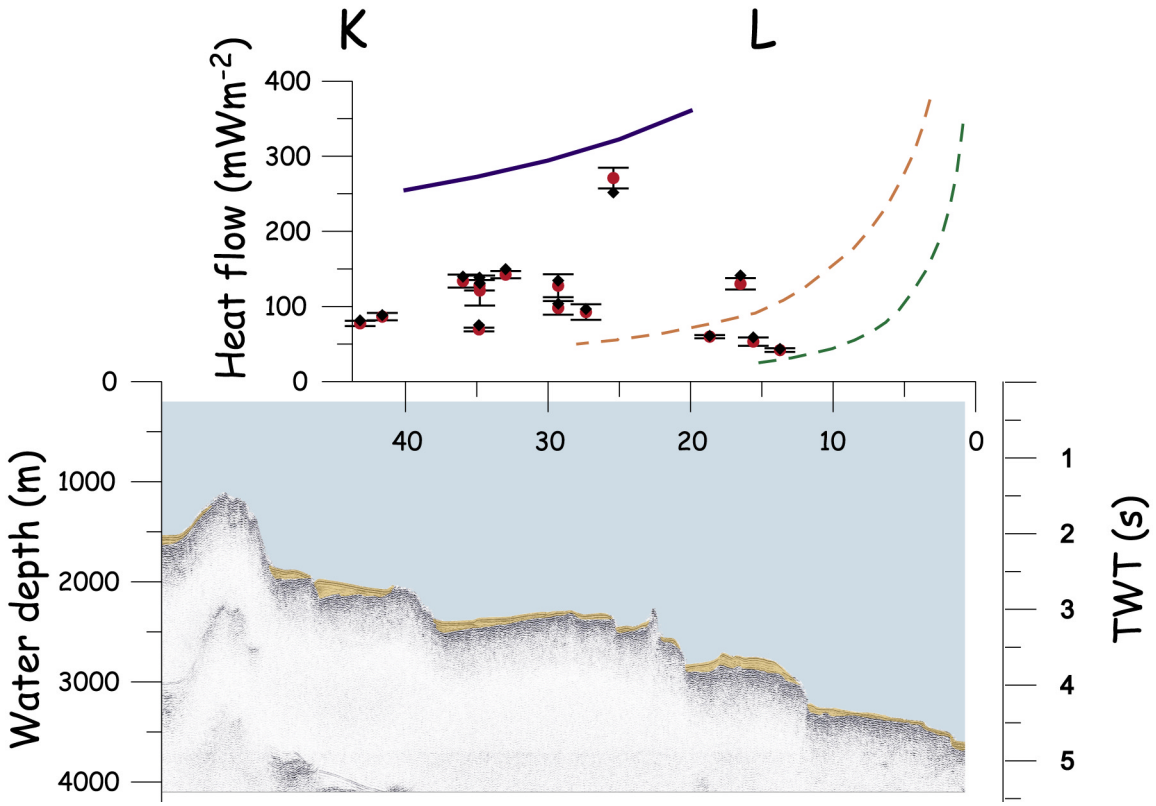

Figure 11. Heat flow measurements (red dots), heat flow corrected for topography and sedimentation (diamonds), HSC conductive model (blue line), Chen and Morgan model (1 cm/year accretion: dashed green line and 3 cm/year accretion: dashed orange line), and seismic profile (sediment cover in yellow) as a function of distance to the ridge axis for profiles KL.

measurements in Profile MN). All measurements except for one heat flow value at 25 km in profile KL (Figure 11) are well below the conductive cooling model predictions (about 25% of the expected value). On profile HG (Figure 6), heat flow seems to increase again at 20 km from the volcanic plateau, in a way similar to that observed on the off-axis domain. It remains relatively low for profile EF, but presents systematic variations along the profile with a wavelength of 10–15 km beneath relative smooth basement, similar to those measured on the Juan de Fuca ridge [*Davis et al.*, 1992].

6. Discussion and Interpretation

[23] The effect of fluid circulation is the most likely cause for the heat flow anomalies described in the previous section, since other causes have been corrected for or are negligible. However, off-axis and near-axis hydrothermal systems are probably different, because of the rapid variation of basal heat flow and the different nature of sediment cover, which is either overall continuous or located on pockets over back-tilted blocks of faulted seafloor. This appears clearly in the nature of heat flow anomalies that are localized off-axis whereas they affect the entire near-axis domain.

[24] The pattern of heat flow anomalies on the eastern flank of the plateau (Figure 9) is consistent with discharge/recharge zones where basement is exposed, as proposed for observations at Juan de Fuca ridge [*Davis et al.*, 1992, 1999; *Stein and Fisher*, 2003]. However, the pattern of circulation is probably not 2-D: for instance, the anomaly that appears near the plateau on profile CD does not exist on profile OP in the same along-axis position with respect to that structure. The distribution of data is however too sparse to infer a 3-D pattern and as a first approximation, we can only interpret heat flow anomalies along profiles. Negative heat flow anomalies on profiles CD and OP are possibly related to lateral flow in a permeable basement below impermeable sediments, where water recharges in the adjacent basement exposures. A quantification of the flow can be obtained with the

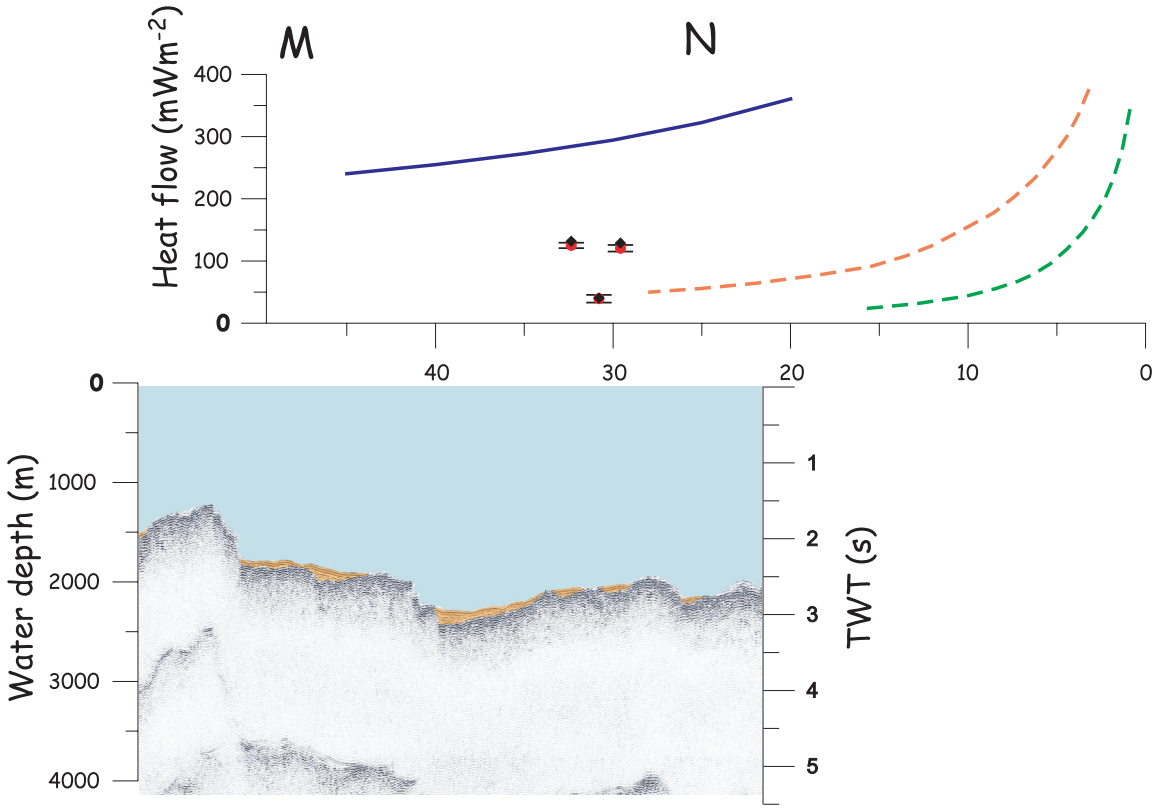

Figure 12. Heat flow measurements (red dots), heat flow corrected for topography and sedimentation (diamonds), conductive model (blue line), Chen and Morgan model (1 cm/year accretion: dashed green line and 3 cm/year accretion: dashed orange line), and seismic profile (sediment cover in yellow) as a function of distance to the ridge axis for profile MN.

simple "heat exchanger" model [*Langseth and Herman*, 1981; *Fisher and Becker*, 2000]. However, the two negative heat flow anomalies would suggest with this model opposite flow directions on profiles CD and OP. The structures that discharge these fluids are not as evident, but may correspond to the positive heat flow anomalies at 105 km on profile CD and 115 km on profile OP.

[25] The "heat exchanger" model can provide a simple analytical solution that relates the magnitude and wavelength of heat flow anomaly to the fluid velocity and the thickness of permeable basement. Inset of Figure 13 shows the geometry assumed by the model: a basement aquifer with thickness h and thermal conductivity λ, overlain by a layer of impermeable sediment with thickness l and thermal conductivity λ_S. The conductive heat flow at base of the aquifer is q_L. Temperature in the aquifer is assumed to be well-mixed, such that the perturbed heat flow is

$$q_m = \lambda_S T(x)/l \tag{1}$$

The energy balance requires that the difference between conductive and surface heat flow is equal to the horizontal heat flow removed by fluids with a Darcy velocity v:

$$h\lambda\frac{\partial^2 T}{\partial x^2} - hv\rho C\frac{\partial T}{\partial x} - q_m + q_L = 0 \tag{2}$$

where ρC is the volumetric specific heat of water.

[26] The solution giving the ratio of measured and conductive heat flow is

$$\frac{q_m}{q_L} = 1 - \exp\left(\frac{-x}{P_e l}\right) \tag{3}$$

P_e is the Peclet number defined by

$$P_e = \frac{vh\rho C}{\lambda_S} \tag{4}$$

The heat flow perturbation can be plotted therefore as a function of distance to the recharge zone, and compared to the model predictions for different parameters values. There is no constraint in the

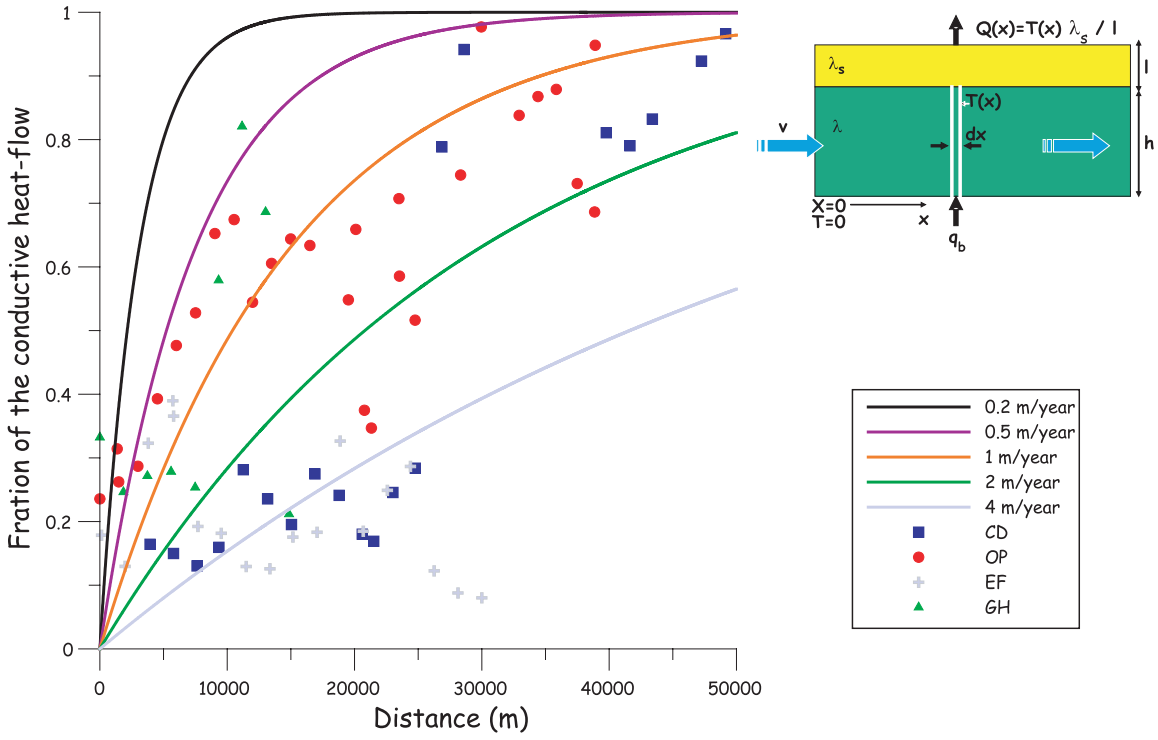

Figure 13. Fraction of the heat flow affected by lateral flow according to the simple heat exchanger model [*Langseth and Herman*, 1981; *Fisher and Becker*, 2000]. h = 500 m, l = 200 m, λ_s = 1 $Wm^{-1}K^{-1}$.

Lucky Strike domain on the thickness of the permeable basement layer, but permeability observed in deep boreholes decreases significantly at depths >500 m below seafloor [*Fisher and Becker*, 2000; *Stein and Fisher*, 2003; *Spinelli et al.*, 2004]. Sediment thickness and thermal conductivity are constrained by local observations. Therefore, assuming that h = 500 m, l = 200 m and λ_S = 1 $Wm^{-1}K^{-1}$, Darcy velocity should be ~1 m/year for profile OP and ~4 m/year for profile CD to satisfy observations (Figure 13). These results are comparable to those at Juan de Fuca [*Davis et al.*, 1999; *Stein and Fisher*, 2003] where the pattern of heat flow and the geometry of basement/sediment are more or less similar to that of profile CD.

[27] *Stein and Fisher* [2003] explored the necessary conditions for free flow with a numerical model that solves for coupled heat and fluid flow. The assumption of hydrostatic conditions necessarily leads to a flow driven toward the ridge axis, according to the topography of isotherms that represents the principal physical cause for instabilities. This is compatible with observations on profile OP only. A reverse flow is suggested for profile CD: this is similar to the pattern observed at Juan de Fuca and discussed by *Stein and Fisher* [2003]. They have obtained a reverse flow only with a condition of permanent cooling in the recharge zone, which is equivalent to imposing denser fluids in the topographic relief. The LUCKYFLUX results suggest that two different systems could coexist very closely and apparently with almost no interaction, but validation of this circulation model will require further constraints (additional heat flow measurements, geochemical data) and 3-D numerical modeling for the specific geometry and thermal conditions.

[28] All measurements near axis are less than the predicted conductive value, but profiles EF and HG, located on the edge of the volcanic plateau limiting off-axis and near-axis domains, show heat flow anomalies also compatible with a lateral flow from the ridge. The "heat exchanger" model applied to those two anomalies suggests flow of the order of 0.5–1 m/year for profile HG and up to 4 m/year for EF (Figure 13). The pattern of anomalies observed on profile EF (Figure 10) reveals in addition systematic variations at a wavelength of ~10–15 km, which could indicate a system of organized convection cells, but would require very high permeability (~10^{-10} m^2), according to the modeling by *Spinelli and Fisher* [2004]. Our results can be compared also to thermal models constrained by independent observa-

tions such as the depth of earthquakes or magma chambers [*Morgan and Chen*, 1993; *Pelayo et al.*, 1994; *Chen and Morgan*, 1996], which integrate a heat balance between magma input and hydrothermal cooling. The model proposed by *Chen and Morgan* [1996], which involves a Nusselt number (ratio between hydrothermal and conductive fluxes) of 8, is in a good agreement with our data (Figures 10, 11, and 12). The overall hydrothermal heat loss in the sediment pockets where we made heat flow measurements could represent therefore between 80 and 90% of the total heat loss. If this value is representative, as the comparison with Chen and Morgan model suggests, of the diffuse heat loss in the Lucky Strike segment (assuming a rift valley floor of ~15 km wide × 100 km long), a total of ~10,000 MW should be discharged at the axis. A part of the discharge is concentrated at hydrothermal vents with maximum flow rates of 0.05 m^3/s [*Lowell and Germanovich*, 1994]. As temperature of Lucky Strike vents ranges between 172–325°C [*Charlou et al.*, 2000], we obtain an upper limit of 50 MW per vent (typically 1 MW, according to *Lowell and Germanovich* [1994]), i.e., 2000–5000 MW for Lucky Strike vent field. As a part of the discharge could be dissipated off-axis and another part by diffusive processes near vent sites [*Becker et al.*, 1996], the magnitude of such vigorous circulation does not appear unreasonable. Additional vent fields unidentified to date may also exist [e.g., *Wilson et al.*, 1996], taking up part of the hydrothermal output.

[29] The observation that hydrothermal processes in the axial domain can transfer up to 90% of the heat flux, whereas it could be almost conductive off-axis is an important outcome of the survey. If this were a general characteristic for the Mid-Atlantic Ridge, it would mean that the importance of off-axis hydrothermal circulation has been overestimated in previous statistical analysis [*Anderson and Skilbeck*, 1981; *Stein and Stein*, 1994]. If not, it would mean that there are some other characteristics in the studied area limiting the effect of hydrothermal circulation: this could be partly explained by the sediment cover, but there is no straightforward relationship. The concept of "hydrothermal sealing" relies however on statistic considerations and might be biased by the nature of previous sites surveyed in the Atlantic. Many of them are located in "unconventional" environments (fracture zones, seamounts vicinity…): the same mode of reasoning applied to LUCKYFLUX data only would give a "sealing age" of ~15 Myr instead of 65 Myr (Figure 14), and on the other hand, there are several sites on oceanic basement where circulation has been identified.

7. Conclusions

[30] The LUCKYFLUX experiment provides more than 150 new heat flow measurements in a MAR segment. We can define two domains of hydrothermal circulation, one near-axis, with overall low heat flow values, and one off-axis, with a large number of heat flow values that are in agreement with conductive models (40% of heat flow values within ±20% of predicted values). These domains are separated by an important topographic structure (a volcanic plateau associated with a V-shaped ridge) that could act as a major component of the hydrodynamic system, where the lack of sediment allows this elevated and rough area to support crustal ventilation.

[31] 1. The axial domain is poorly characterized owing to problems in penetration of the heat flow probe, and to the uneven distribution of sediment. However, heat flow measurements can be interpreted in term of water flow driven from the flank toward the ridge axis. In some places, wavelengths of 10–15 km in surface heat flow, with no relation to basement geometry or sediment thickness, can suggest that large-scale hydrothermal circulation could be broken in smaller cells. Our results are generally in agreement with the *Chen and Morgan* [1996] model that predict a heat flux that is 90% hydrothermal.

[32] 2. The off-axis domain shows a complex surface pattern of positive and negative heat flow anomalies. Heat flow anomalies are mostly located near basement exposures, but basement structures are not always associated with anomalies. Smaller size characterizes positive anomalies, and two major negative anomalies of opposite geographic polarity can be defined. The first is located at the eastern flank of the plateau, which may imply heat moving from west to east. The second is located near a basement exposure at the east of the surveyed region, which may suggest a significant transfer from east to west.

[33] First-order modeling requires fluid velocities comparable to that proposed for Juan de Fuca (order of 1–10 m/year for 500 m of highly permeable basement). This suggests that the permeability structure is comparable in slow (MAR) and intermediate spreading-rate ridge environments. This is based on the interpretation of heat flow data with a simple aquifer model, and would of course needs further evidences (e.g., analysis of chemical spe-

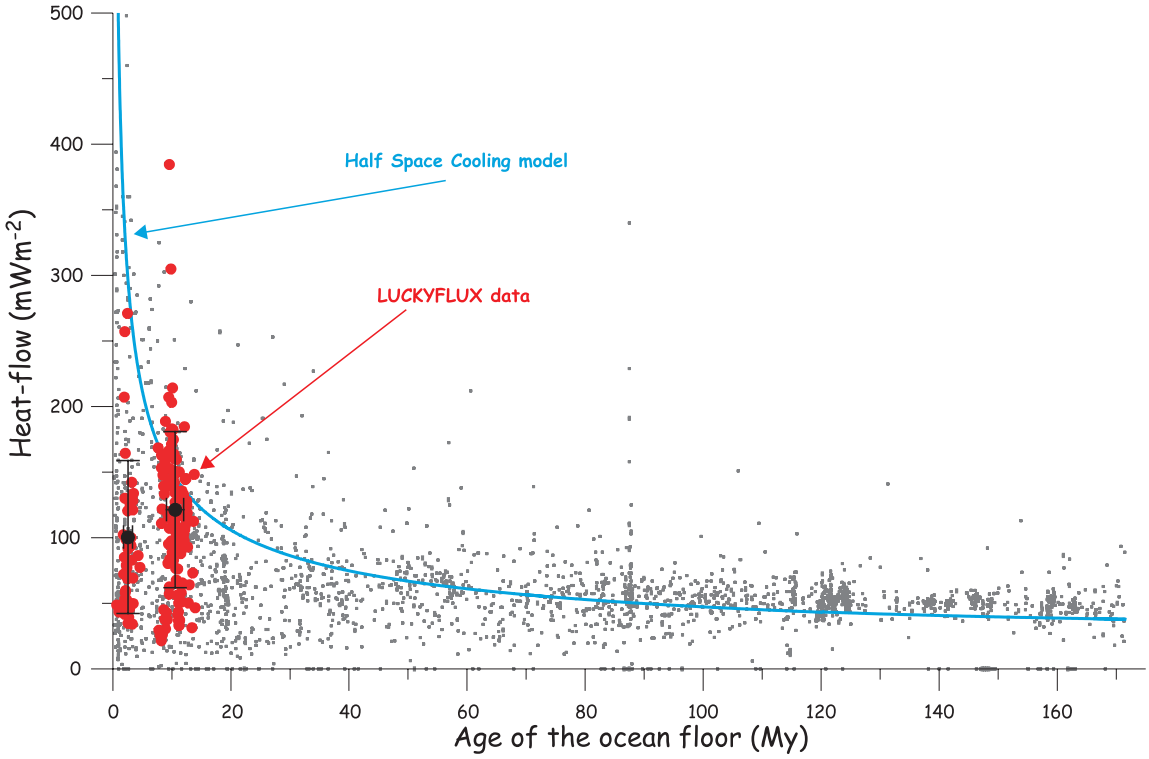

Figure 14. Heat flow versus age of the ocean floor for the Atlantic Ocean. LUCKYFLUX data and their average off-axis (121 ± 59 mWm^{-2}) and near-axis (100 ± 58 mWm^{-2}) values are also reported.

cies in presumed hydrothermal systems) and further modeling to explore the 3-D configuration.

[34] One important result of this study is that 40% of the off-axis measurements (and perhaps more in terms of area involved) are near the predicted conductive values. This suggests, in addition to observations of hydrothermal systems in old oceanic basement elsewhere, that the "sealing age" concept of *Stein and Stein* [1994] is mostly dependent on the nature of surveyed sites (sediment cover, density of seamounts, tectonic context...) rather than age alone and probably not directly relevant for the permeability structure of the crust.

Appendix A

A1. Topographic Corrections

[35] The presence of irregular topography at the Earth surface can perturb the distribution of shallow depths isotherms, which are otherwise horizontal. A general consequence is that heat flow appears higher (lower) where depressions (highs) exist. Where accurate topographic information exists, systematic corrections can be determined. In the marine environment, it has rarely been applied because the resolution of available bathymetry is usually insufficient, although the effect can be important where canyons or seamounts exist. For example, large edge effects have been recognized in the vicinity of Congo submarine channel [*Lucazeau et al.*, 2004]. A correction for non-level terrain proposed by *Bullard* [1940] assumes that the topographic variations are small enough that the temperature differences δT in the plane $z = -h_0$ (elevation at the measurement location) are assumed linearly proportional to z:

$$\delta T(x,y,-h_0) = (G - G')(h(x,y) - h_0) \qquad \text{(A1)}$$

where G is the undisturbed gradient in the ground and G′ the temperature gradient in water. δT follows the Laplace equation, and can be continued downward:

$$\delta T(x,y,z) = \frac{G - G'}{2\pi} \int_{-\infty}^{+\infty} \int \cdot \frac{(h(x',y') - h_0)(z + h_0)dx'dy'}{\left((x-x')^2 + (y-y')^2 + (z+h_0)^2\right)^{3/2}} \qquad \text{(A2)}$$

We used the practical method proposed by *Kappelmeyer and Haenel* [1974], and averaged

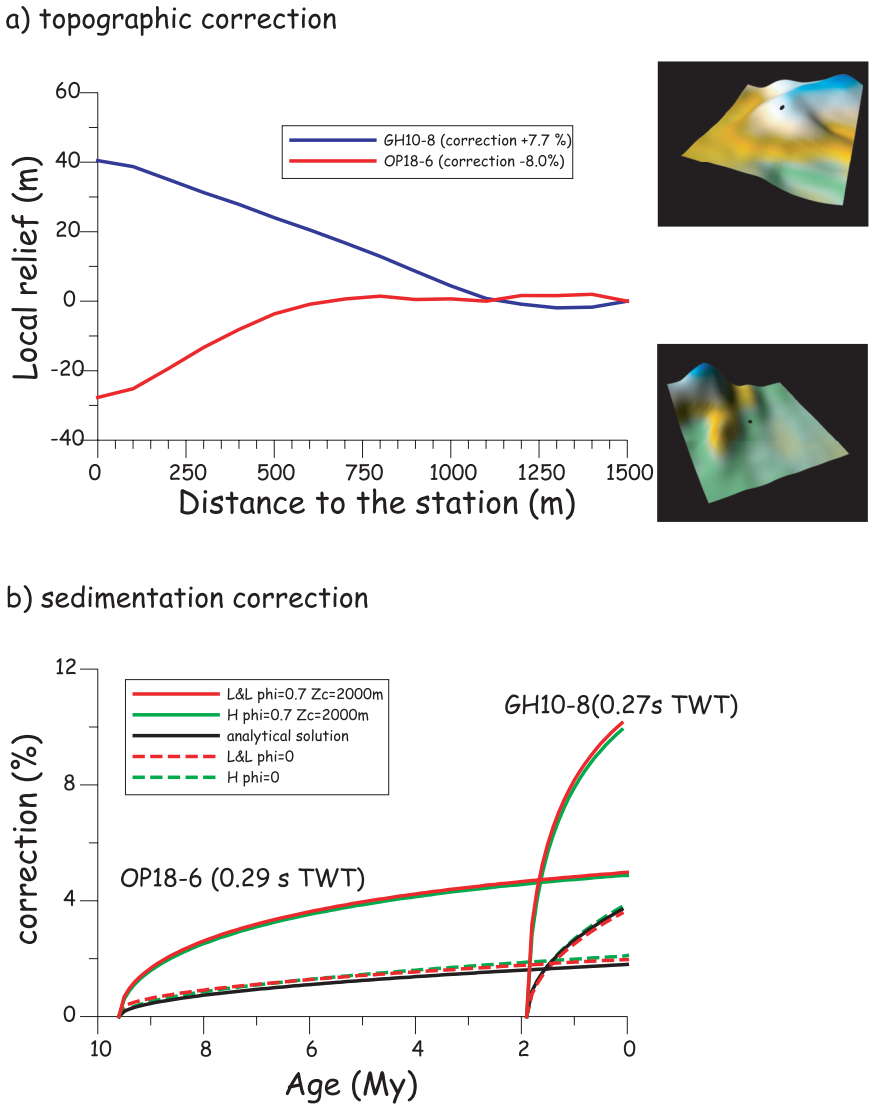

Figure A1. Examples of applied corrections. (a) Average topographic profiles around stations with the highest positive (GH10-8) and negative (OP18-6) corrections. Corresponding digital elevation models around stations are displayed (box size is 3000 meters wide). (b) For the same stations, sedimentation corrections obtained with an analytical solution and numerical solutions (L&L [*Lucazeau and Le Douaran*, 1985] and H [*Hutchinson*, 1985]) that include compaction of sediment, sediment heat production, and effects of compaction and temperature on sediment conductivity. Hutchinson's model includes effect of compaction fluids advection.

the bathymetry on circular sectors around individual heat flow measurement location. We have chosen a 2-km diameter sector, and used available multibeam bathymetry gridded at 100 m. This correction is usually small (1–2%) but may reach (8%) when local relief exists near the measurement location (see Figure A1 and Table 1).

A2. Sediment Corrections

[36] Sediment deposited on the seafloor at initially uniform bottom water temperatures reduces the heat flow measured at the Earth surface compared to deeper values. The importance of the perturbation depends mostly on the sedimentation rate and duration, which can be estimated from the thickness of sediment and age of ocean floor both reported in Table 1. Sedimentation or erosion is a classical problem of heat conduction in a moving medium [*Carslaw and Jaeger*, 1959, p. 387; *Turcotte and Schubert*, 1982, p. 174], for which a simple analytical correction has been given by *Von Herzen et al.* [1974].

[37] However, this analytical solution does not include such important effects as variable sedimen-

tation rates, compaction and its effect on thermal conductivity, or the thermal interaction with basement for high sedimentation rates [*Hutchinson*, 1985; *Lucazeau and Le Douaran*, 1985; *Von Herzen et al.*, 1989; *Harris et al.*, 2000]. Numerical solutions can solve this problem, and algorithms have been proposed by *Hutchinson* [1985] and *Lucazeau and Le Douaran* [1985]. Although the two algorithms use different strategies and hypothesis, both give very similar results (within 0.5% of heat flow anomaly). Compaction is considered in both models as a function of porosity, which is assumed to decrease exponentially with depth. At the limit where surface porosity is equal to zero (no compaction), both models are in agreement with the analytical solution provided by *Von Herzen et al.* [1974]. Corrections including compaction are up to three times higher than the analytical method (Figure A1b). This difference is related mostly to the thermal blanketing of sediment, which delays the dissipation of the perturbation, whereas the heat advection related to the fluid expulsion due to compaction is rather limited.

[38] Sediment thickness has been picked as two-way travel time (TWT) on seismic profiles acquired during a previous survey (SUDAÇORES). Heat flow profiles are on the trace of seismic lines, except for profiles AB and OP, for which the sediment thickness is interpolated from adjacent seismic data. The maximum TWT thickness reaches 0.7 s (Table 1) and, assuming a velocity range of 1500–2000 m/s, corresponds to a 525–700 m thick sediment cover. The heat flow correction due to sedimentation has been computed for the upper limit (2000 m/s), and is therefore a maximum estimate. Resulting sedimentation rates are therefore 30–40 m/Myr for off-axis profiles and can reach 100–150 m/Myr for some profiles in the axial domain. These sedimentation rates are local rates and have obviously no significance on a regional scale. They can affect however the magnitude of heat flow by 5% (with a maximum of 15%) when the compaction is included (assuming surface porosity = 0.7, compaction length scale = 2000 m and bulk surface conductivity = 1 $Wm^{-1}K^{-1}$).

A3. Heat Refraction

[39] The contrast of conductivity between sediment (~0.8–1 W/m/K) and basalt (~1.5–2.5 W/mK) [*Clauser and Huenges*, 1995] can potentially contribute to a lateral heat transfer. This heat refraction effect, which has been shown to be important in some specific environments [*Nagihara et al.*, 1992], could generate small wavelength anomalies such as that observed on profile OP or profile CD, where the basement shows a high bounded by two lows. *Von Herzen* [2004] has discussed some aspect of heat refraction for buried structures in the old ocean crust. In the present study, we have several measurements near small seamounts, which may cause different perturbations. These seamounts appear sometimes in the high-resolution bathymetric map, but not on seismic profiles that have a larger spacing than the wavelength of the seamounts. A systematic correction is therefore difficult, but the expected magnitude of heat refraction can be modeled for simple geometries. We prescribed Gaussian-shape structures onlapped by sediments (inset of compaction fluids advection.

[40] Figure A2: This is convenient to test the wavelength and amplitude variations. The heat equation was solved with a 2-D finite element code for a stationary regime, constant heat flow at 5 km depth, and no heat flow through the vertical boundaries. The mesh includes 200 * 20 4-nodes isoparametric elements. When the structure is at the same level as the sediment, there is a smooth increase of heat flow with a maximum at the structure center, which depends on basement wavelength, contrasts of conductivity between basement and sediments, thickness of sediments.

[41] Figure A2a: For the most realistic sets of parameters, the effect does not exceed 50% ($Q/Q_0 < 1.5$). However, when the basement emerges from the sediment, there is a very short wavelength (~0.1 a) high amplitude anomalies (2–4 times Q_0) at the transition between basement and sediment. Heat refraction cannot be excluded where isolated positive anomalies are observed, but water discharges appear more likely where several consecutive measurements exist (e.g., profile CD at 105 km and profile OP at 118 km).

A4. Temporal Stability of Bottom Water Temperature

[42] The accuracy of heat flow measurements obtained with shallowly penetrating probes depends strongly on the bottom water temperature stability. *Davis et al.* [2003] have reported stable long term records of near bottom temperature in the central Atlantic near the Mid Oceanic Ridge (at ODP CORK site 395, 22°45N–46°04W), while

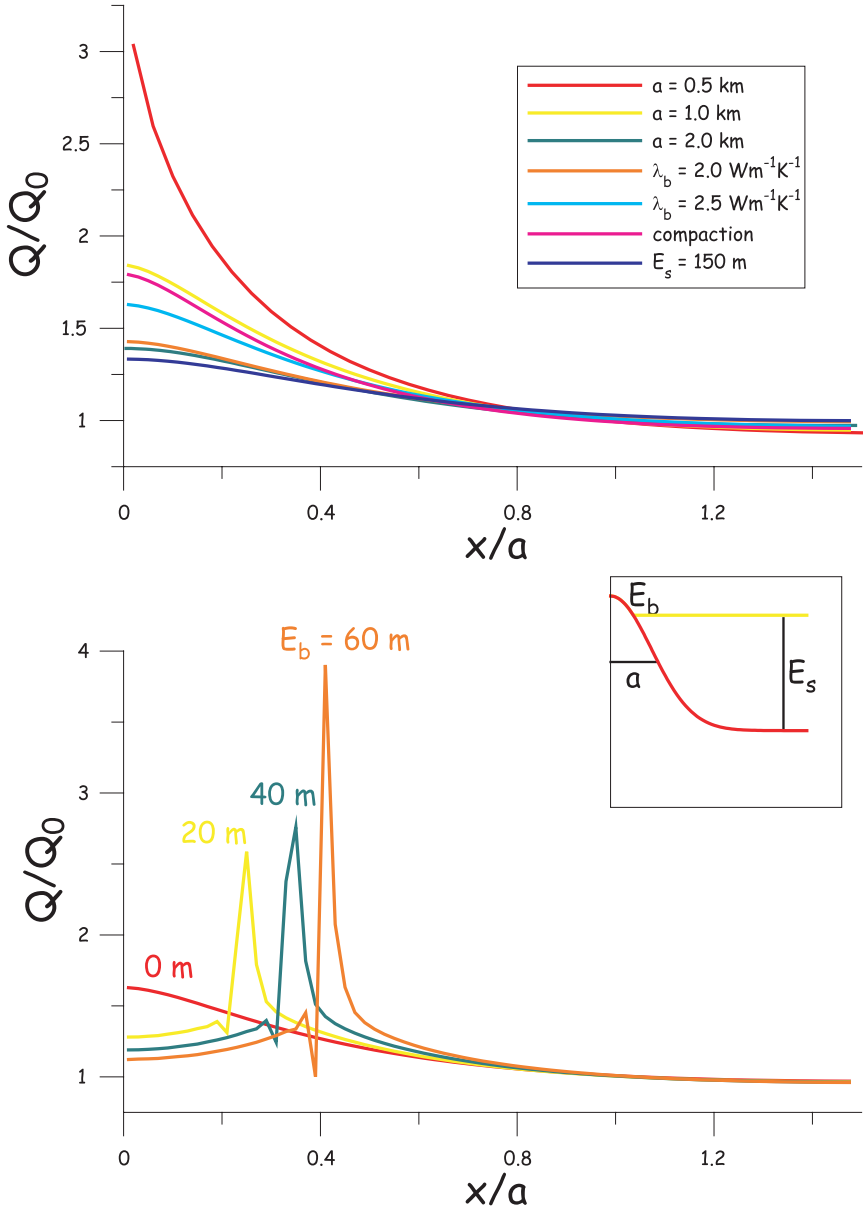

Figure A2. Heat refraction effect for a Gaussian-shape basement structure plotted as the normalized heat flow versus normalized distance. (a) Basement and sediment at the same elevation. The reference parameters are a = 1 km (Gaussian width), $\lambda_s = 1$ $Wm^{-1}K^{-1}$, $\lambda_b = 3$ $Wm^{-1}K^{-1}$, and $E_s = 300$ m. (b) Basement emerges from the sediment by an amount E_b. $E_s = 300$ m.

similar conclusions have been drawn by *Thurnherr et al.* [2002] for the Azores area. The mostly linear gradients determined during the Lucky Flux measurements (Figure 4) confirm that large variations of near bottom temperatures are unlikely to have occurred in recent times. In addition, water temperatures (Table 1) show remarkable trends. In the axial zone, they are significantly higher (around 4°C) and do not vary importantly with depth. This relative stability has been interpreted by *Thurnherr et al.* [2002] as consequence of the confined axial domain and high geothermal heat flow area. Off-axis, water temperatures decrease with increasing depth as may be expected for a stably stratified ocean, with the exception of a few locations on profile CD, which surprisingly coincide with edges of heat flow anomalies where bottom water temperatures increase significantly with no important change in-depth (see in Table 1 stations 6-5, 6-8, 6-16, and 8-1 and Figure A3). These locations could

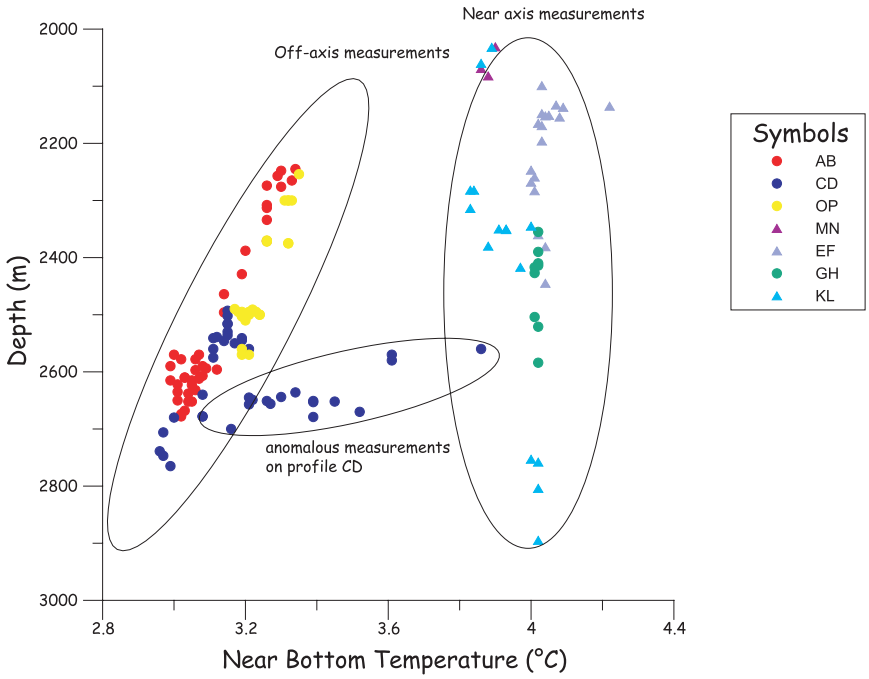

Figure A3. Near bottom temperatures recorded during the LUCKY FLUX experiment.

be a manifestation of local vertical water flow through sediment fractures.

Acknowledgments

[43] We want to thank the officers and crew of the POSEIDON, who conducted smooth operations throughout the LUCKYFLUX Cruise. Funding for the cruise was provided by the French Ministère de la Recherche. The heat flow equipment was originally developed at Woods Hole Oceanographic Institution and refurbished at the Institut de Physique du Globe. Earl Davis and an anonymous reviewer helped to clarify the concepts and presentation of this paper. Contribution IPGP 2129.

References

Anderson, R. N., and J. N. Skilbeck (1981), Oceanic heat flow, in *The Oceanic Lithosphere*, vol. 7, *The Seas*, edited by C. Emiliani, pp. 489–523, Wiley-Interscience, Hoboken, N. J.

Anderson, R. N., M. G. Langseth, and M. A. Hobart (1979), Geothermal convection through oceanic crust and sediments in the Indian Ocean, *Science*, *204*, 828–832.

Becker, K., R. V. Herzen, J. Kirklin, R. Evans, D. Kadko, M. Kinoshita, O. Matsubayashi, R. Mills, A. Schultz, and P. Rona (1996), Conductive heat flow at the TAG active hydrothermal mound: Results from 1993–1995 submersible surveys, *Geophys. Res. Lett.*, *23*(23), 3463–3466.

Birch, F. S., and A. J. Halunen (1966), Heat flow measurements in the Atlantic ocean, Indian ocean, Mediterranean sea and Red Sea, *J. Geophys. Res.*, *71*(B2), 583–586.

Bonneville, A., R. P. Von Herzen, and C. Ruppel (1993), HFsoft: Toolbox for processing marine heat flow data acquired with MCHF instrumentation, 54 pp., *Tech. Memo. WHOI-02–93*, Woods Hole Oceanogr. Inst., Woods Hole, Mass.

Bullard, E. C. (1940), The disturbance of the temperature gradient in the Earth's crust by inequalities of height, *Mon. Not. R. Astron. Soc. Geophys. Suppl.*, *4*, 300–362.

Bullard, E. C. (1954), The flow of heat through the floor of the Atlantic Ocean, *Proc. R. Soc. London, Ser. A*, *222*, 408–429.

Bullard, E. C., and A. Day (1961), The flow of heat through the floor of the Atlantic Ocean, *Geophys. J. R. Astron. Soc.*, *4*, 282–292.

Cannat, M., A. Briais, C. Deplus, J. Escartin, J. Georgen, J. Lin, S. Mercouriev, C. Meyzen, M. Muller, and G. Pouliquen (1999), Mid-Atlantic Ridge-Azores hotspot interactions: Along-axis migration of a hotspot-derived event of enhanced magmatism 10 to 4 Ma ago, *Earth Planet. Sci. Lett.*, *173*(3), 257–269.

Carslaw, H. S., and J. C. Jaeger (1959), *Conduction of Heat in Solids*, 510 pp., Oxford Univ. Press, New York.

Charlou, J. L., J. P. Donval, E. Douville, P. Jean-Baptiste, J. Radford-Knoery, Y. Fouquet, A. Dapoigny, and M. Stievenard (2000), Compared geochemical signatures and the evolution of Menez Gwen (37°50′N) and Lucky Strike (37°17′N) hydrothermal fluids, south of the Azores Triple Junction on the Mid-Atlantic Ridge, *Chem. Geol.*, *171*(1–2), 49–75.

Chen, Y. J., and J. P. Morgan (1996), The effects of spreading rate, the magma budget, and the geometry of magma emplacement on the axial heat flux at mid-ocean ridges, *J. Geophys. Res.*, *101*(B5), 11,475–11,482.

Clauser, C., and E. Huenges (1995), Thermal conductivity of rocks and minerals, in *Rock Physics and Phase Relations: A Handbook of Physical Constants*, *AGU Ref. Shelf Ser.*, vol. 3, edited by T. J. Ahrens, pp. 105–126, AGU, Washington, D. C.

Davis, E. E., D. S. Chapman, C. B. Forster, and H. Villinger (1989), Heat-flow variations correlated with buried basement topography on the Juan de Fuca Ridge, *Nature*, *342*, 533–537.

Davis, E. E., et al. (1992), Flankflux: An experiment to study the nature of hydrothermal circulation in young oceanic crust, *Can. J. Earth Sci.*, *29*, 925–952.

Davis, E. E., D. S. Chapman, K. Wang, H. Villinger, A. T. Fisher, S. W. Robinson, J. Grigel, D. Pribnow, J. Stein, and K. Becker (1999), Regional heat flow variations across the sedimented Juan de Fuca Ridge eastern flank: Constraints on lithospheric cooling and lateral hydrothermal heat transport, *J. Geophys. Res.*, *104*(B8), 17,675–17,688.

Davis, E. E., K. Wang, K. Becker, R. E. Thomson, and I. Yashayaev (2003), Deep-ocean temperature variations and implications for errors in seafloor heat flow determinations, *J. Geophys. Res.*, *108*(B1), 2034, doi:10.1029/2001JB001695.

Detrick, R. S., H. D. Needham, and V. Renard (1995), Gravity anomalies and crustal thickness variations along the Mid-Atlantic Ridge between 33°N and 40°N, *J. Geophys. Res.*, *100*, 3767–3787.

Embley, R. W., M. A. Hobart, R. N. Anderson, and D. H. Abbott (1983), Anomalous heat flow in the northwest Atlantic: A case for continued hydrothermal circulation in 80 My crust, *J. Geophys. Res.*, *88*(B2), 1067–1074.

Escartín, J., M. Cannat, G. Pouliquen, A. Rabain, and J. Lin (2001), Crustal thickness of V-shaped ridges south of the Azores: Interaction of the Mid-Atlantic Ridge (36°–39°N) and the Azores hot spot, *J. Geophys. Res.*, *106*(B10), 21,719–21,736.

Fisher, A. T., and K. Becker (2000), Channelized fluid flow in oceanic crust reconciles heat-flow and permeability data, *Nature*, *403*(6765), 71–74.

Fisher, A. T., et al. (2003), Hydrothermal recharge and discharge across 50 km guided by seamounts on a young ridge flank, *Nature*, *421*(6923), 618–621.

Foster, S. E., G. Simmons, and W. Lamb (1974), Heat-flow near a North Atlantic fracture zone, *Geothermics*, *3*, 3.

Gente, P., J. Dyment, M. Maia, and J. Goslin (2003), Interaction between the Mid-Atlantic Ridge and the Azores hot spot during the last 85 Myr: Emplacement and rifting of the hot spot-derived plateaus, *Geochem. Geophys. Geosyst.*, *4*(10), 8514, doi:10.1029/2003GC000527.

Green, K. E., R. P. Von Herzen, and D. L. Williams (1981), The Galapagos spreading center at 86°W: A detailed geothermal field study, *J. Geophys. Res.*, *86*, 979–986.

Harris, R. N., G. Garven, J. Georgen, M. K. McNutt, L. Christiansen, and R. P. Von Herzen (2000), Submarine hydrogeology of the Hawaiian archipelagic apron: 1. Heat flow patterns north of Oahu and Maro Reef, *J. Geophys. Res.*, *105*(B9), 21,371–21,386.

Hutchinson, I. (1985), The effects of sedimentation and compaction on oceanic heat flow, *Geophys. J. R. Astron. Soc.*, *82*, 439–459.

Hyndman, R. D., and D. S. Rankin (1972), The Mid-Atlantic Ridge near 45 N. XVIII. Heat flow measurements, *Can. J. Earth Sci.*, *8*, 664–670.

Hyndman, R. D., R. P. Von Herzen, A. J. Erickson, and J. Jolivet (1976), Heat flow measurements in deep crustal holes on the Mid-Atlantic Ridge, *J. Geophys. Res.*, *81*, 4053–4060.

Kappelmeyer, O., and R. Haenel (1974), *Geothermics With Special Reference to Application*, 238 pp., Gebr. Borntraeger, Berlin.

Kasameyer, P. W., R. P. Von Herzen, and G. Simmons (1972), Heat flow, bathymetry and the Mid-Atlantic Ridge at 43 N, *J. Geophys. Res.*, *77*, 2535–2542.

Langseth, M. G., and B. J. Herman (1981), Heat transfer in the oceanic crust of the Brazil basin, *J. Geophys. Res.*, *86*, 10,805–10,819.

Langseth, M. G., X. Le Pichon, and M. Ewing (1966), Crustal structure of the mid-ocean ridges: 5. Heat flow through the Atlantic Ocean floor and convection currents, *J. Geophys. Res.*, *71*, 5321–5355.

Langseth, M. G., M. J. Mottl, M. A. Hobart, and A. T. Fisher (1988), The distribution of geothermal and geochemical gradients near Site 501/504: Implications for hydrothermal circulation in the oceanic crust, *Proc. Ocean Drill. Program Initial Rep.*, *111*, 23–32.

Lister, C. R. B. (1972), On the thermal balance of a mid-ocean ridge, *Geophys. J. R. Astron. Soc.*, *26*, 515–535.

Lowell, R. P., and L. N. Germanovich (1994), On the temporal evolution of high-temperature hydrothermal systems at ocean ridge crests, *J. Geophys. Res.*, *99*(B1), 565–576.

Lucazeau, F., and S. Le Douaran (1985), The blanketing effect of sediments in basins formed by extension: A numerical model. Application to the Gulf of Lion and the Viking graben, *Earth Planet. Sci. Lett.*, *74*(1), 92–102.

Lucazeau, F., F. Brigaud, and J. L. Bouroullec (2004), High-resolution heat flow density in the lower Congo basin, *Geochem. Geophys. Geosyst.*, *5*, Q03001, doi:10.1029/2003GC000644.

Morgan, J. P., and Y. J. Chen (1993), The genesis of oceanic crust: Magma injection, hydrothermal circulation, and crustal flow, *J. Geophys. Res.*, *98*(B4), 6283–6298.

Nagihara, S., J. G. Sclater, L. M. Beckley, E. W. Behrens, and L. A. Lawver (1992), High heat flow anomalies over salt structures on the Texas continental slope, Gulf of Mexico, *Geophys. Res. Lett.*, *19*(16), 1687–1690.

Parsons, B., and J. G. Sclater (1977), An analysis of the variation of ocean floor bathymetry and heat flow with age, *J. Geophys. Res.*, *82*, 803–827.

Pelayo, A. M., S. Stein, and C. S. Stein (1994), Estimation of oceanic hydrothermal heat flux from heat flow and depths of midocean ridge seismicity and magma chambers, *Geophys. Res. Lett.*, *21*(8), 713–716.

Phillips, J. D., R. P. Thompson, R. P. Von Herzen, and V. T. Bowen (1969), Mid-Atlantic Ridge near 43 N Latitude, *J. Geophys. Res.*, *74*, 3069–3081.

Pollack, H. N., S. J. Hurter, and J. R. Johnston (1993), Heat loss from the Earth's interior: Analysis of the global data set, *Rev. Geophys.*, *31*, 267–280.

Sclater, J. G. (2003), Earth science: Ins and outs on the ocean floor, *Nature*, *421*(6923), 590–591.

Sclater, J. G., and J. Francheteau (1970), The implication of terrestrial heat flow: Observations on current tectonic and geochemical models of the crust and upper mantle of the Earth, *Geophys. J. R. Astron. Soc.*, *20*, 509–542.

Spinelli, G. A., L. Zühlsdorff, A. T. Fisher, C. G. Wheat, M. Mottl, V. Spieß, and E. R. Giambalvo (2004), Hydrothermal seepage patterns above a buried basement ridge, eastern flank of the Juan de Fuca Ridge, *J. Geophys. Res.*, *109*, B01102, doi:10.1029/2003JB002476.

Stein, C. S., and S. Stein (1992), A model for the global variation in oceanic depth and heat flow with lithospheric age, *Nature*, *359*, 123–129.

Stein, C. S., and S. Stein (1994), Constraints on hydrothermal heat flux through the oceanic lithosphere from global heat flow, *J. Geophys. Res.*, *99*(B2), 3081–3096.

Stein, J. S., and A. T. Fisher (2003), Observations and models of lateral hydrothermal circulation on a young ridge flank: Numerical evaluation of thermal and chemical constraints, *Geochem. Geophys. Geosyst.*, *4*(3), 1026, doi:10.1029/2002GC000415.

Thomson, R. E., E. E. Davis, and B. J. Burd (1995), Hydrothermal venting and geothermal heating in Cascadia Basin, *J. Geophys. Res.*, *100*(B4), 6121–6142.

Thurnherr, A. M., K. J. Richards, C. R. German, G. F. Lane-Serff, and K. G. Speer (2002), Flow and mixing in the Rift Valley of the Mid-Atlantic Ridge, *J. Phys. Oceanogr.*, *32*, 1763–1778.

Turcotte, D. L., and G. Schubert (1982), *Geodynamics: Applications of Continuum Physics to Geological Problems*, 450 pp., John Wiley, Hoboken, N. J.

Villinger, H., I. Grevemeyer, N. Kaul, J. Hauschild, and M. Pfender (2002), Hydrothermal heat flux through aged oceanic crust: Where does the heat escape?, *Earth Planet. Sci. Lett.*, *202*(1), 159–170.

Von Herzen, R. P. (1987), Measurement of oceanic heat flow, in *Methods of Experimental Physics-Geophysics*, edited by C. Sammis and T. L. Henyey, pp. 227–263, Elsevier, New York.

Von Herzen, R. P. (2004), Geothermal evidence for continuing hydrothermal circulation in older (>60 M.y.) ocean crust, in *Hydrogeology of the Oceanic Lithosphere*, edited by E. E. Davis and H. Elderfield, pp. 414–447, Cambridge Univ. Press, New York.

Von Herzen, R. P., P. Finckh, and K. J. Hsu (1974), Heat flow measurements in Swiss lakes, *J. Geophys. Res.*, *40*, 141–172.

Von Herzen, R. P., M. J. Cordery, R. S. Detrick, and C. Fang (1989), Heat flow and the thermal origin of hotspot swells: The Hawaiian swell revisited, *J. Geophys. Res.*, *94*, 13,783–13,799.

Wheat, C. G., M. J. Mottl, A. T. Fisher, D. Kadko, E. E. Davis, and E. Baker (2004), Heat flow through a basaltic outcrop on a sedimented young ridge flank, *Geochem. Geophys. Geosyst.*, *5*, Q12006, doi:10.1029/2004GC000700.

Williams, D. L., R. P. Von Herzen, J. G. Sclater, and R. N. Anderson (1974), The Galapagos spreading centre: Lithospheric cooling and hydrothermal circulation, *Geophys. J. R. Astron. Soc.*, *38*, 587–608.

Williams, D. L., T. C. Lee, R. P. Von Herzen, K. E. Green, and M. A. Hobart (1977), A geothermal study of the Mid-Atlantic Ridge near 37°N, *Bull. Geol. Soc. Am.*, *88*, 531–540.

Wilson, C., J. L. Charlou, E. Ludford, G. Klinkhammer, C. Chin, H. Bougault, C. R. German, K. G. Speer, and M. Palmer (1996), Hydrothermal anomalies in the Lucky Strike segment on the Mid-Atlantic Ridge (37°17′N), *Earth Planet. Sci. Lett.*, *142*, 467–477.